

Morphological Butcher-Oemler effect in the SDSS Cut & Enhance Galaxy Cluster Catalog

Tomotsugu GOTO^{1,2,3}, Sadanori OKAMURA², Masafumi YAGI⁴, Ravi K. SHETH⁵,
Neta A. BAHCALL⁶, Shane A. ZABEL⁷, Michael S. CROUCH⁷, Maki SEKIGUCHI¹,
James ANNIS⁸, Mariangela BERNARDI⁷, Shang-Shan CHONG⁷, Percy L. GÓMEZ⁷,
Sarah HANSEN⁹, Rita S. J. KIM¹⁰, Adam KNUDSON⁷, Timothy A. MCKAY⁹,
and Christopher J. MILLER⁷

¹*Institute for Cosmic Ray Research, University of Tokyo,
Kashiwanoha, Kashiwa, Chiba 277-0882, Japan*

²*Department of Astronomy and Research Center for the Early Universe,
School of Science, University of Tokyo, Tokyo 113-0033, Japan*

³*yohnis@icrr.u-tokyo.ac.jp*

⁴*National Astronomical Observatory, 2-21-1 Osawa, Mitaka, Tokyo 181-8588, Japan.*

⁵*Department of Physics and Astronomy University of Pittsburgh
3941 O'Hara Street Pittsburgh, PA 15260*

⁶*Princeton University Observatory, Princeton, NJ 08544, USA*

⁷*Department of Physics, Carnegie Mellon University,
5000 Forbes Avenue, Pittsburgh, PA 15213-3890, USA*

⁸*Fermi National Accelerator Laboratory, P.O. Box 500, Batavia, IL 60510, USA*

⁹*University of Michigan, Department of Physics,
500 East University, Ann Arbor, MI 48109, USA*

¹⁰*Department of Physics and Astronomy, The Johns Hopkins University,
3400 North Charles Street, Baltimore, MD 21218-2686, USA*

(Received ; accepted)

Abstract

We investigate the evolution of the fractions of late type cluster galaxies as a function of redshift, using one of the largest, most uniform cluster samples available. The sample consists of 514 clusters of galaxies in the range $0.02 \leq z \leq 0.3$ from the Sloan Digital Sky Survey Cut & Enhance galaxy cluster catalog. This catalog was created using a single automated cluster finding algorithm applied to uniform data from a single telescope, with accurate CCD photometry, thus, minimizing selection biases. We use four independent methods to analyze the evolution of the late type galaxy fraction. Specifically, we select late type galaxies based on: restframe $g-r$ color, $u-r$ color, galaxy profile fitting and concentration index. The first criterion corresponds to

the one used in the classical Butcher-Oemler analyses. The last two criteria are more sensitive to the morphological type of the galaxies. In all the four cases, we find an increase in the fraction of late type galaxies with increasing redshift, significant at the 99.9% level. The results confirm that cluster galaxies do change colors with redshift (the Butcher-Oemler effect) and, in addition, they change their morphology to later-type toward higher redshift — indicating a morphological equivalent of the Butcher-Oemler effect. We also find a tendency of richer clusters to have lower fractions of late type galaxies. The trend is consistent with a ram pressure stripping model, where galaxies in richer clusters are affected by stronger ram pressure due to higher temperature of clusters.

Key words: galaxies: clusters: general

1. Introduction

The Butcher-Oemler effect was first reported by Butcher & Oemler (1978, 1984) as an increase in the fraction of blue galaxies (f_b) toward higher redshift in 33 galaxy clusters over the redshift range $0 < z < 0.54$. Butcher and Oemler’s work made a strong impact since it showed direct evidence for the evolution of cluster galaxies. Much work regarding the nature of these blue galaxies followed. Rakos & Schombert (1995) found that the fraction of blue galaxies increases from 20% at $z=0.4$ to 80% at $z=0.9$, suggesting that the evolution in clusters is even stronger than previously thought. Margoniner & De Carvalho (2000) studied 48 clusters in the redshift range of $0.03 < z < 0.38$ and detected a strong Butcher-Oemler effect consistent with that of Rakos & Schombert (1995). Despite the trend with redshift, almost all previous work has reported a wide range of blue fraction values. In particular, in a large sample of 295 Abell clusters, Margoniner et al. (2001) not only confirmed the existence of the Butcher-Oemler effect, but also found the blue fraction depends on cluster richness.

Although the detection of the Butcher-Oemler effect has been claimed in various studies, there have been some suggestions of strong selection biases in the cluster samples. Newberry, Kirshner & Boroson (1988) measured velocity dispersions and surface densities of galaxies in clusters and found a marked difference between local clusters and intermediate redshift clusters. More recently, Andreon & Ettori (1999) measured X-ray surface brightness profiles, sizes, and luminosities of the Butcher-Oemler sample of clusters and concluded that the sample is not uniform. The selection bias, thus, could mimic evolutionary effects. Smail et al. (1998) used 10 X-ray bright clusters in the redshift range of $0.22 \leq z \leq 0.28$ and found that the clusters have only a small fraction of blue galaxies. The Butcher-Oemler effect was not observed with their sample. Similarly, galaxies in radio selected groups are not significantly bluer at higher redshifts (Allington-Smith et al. 1993). Garilli et al. (1996) observed 67 Abell and X-ray selected clusters

and found no detectable Butcher-Oemler effect until $z=0.2$. Fairley et al. (2002) studied eight X-ray selected galaxy clusters and found no correlation of blue fraction with redshift. Rakos & Schombert (1995)'s sample were selected from the catalog compiled by Gunn, Hoessel & Oke (1986) using photographic plates taken only in two color bands. The sample thus have a possible bias against red, high redshift clusters. In addition to the possible sample selection biases, with the exception of Margoniner et al. (2001), the number of clusters in the previous works was small, consisting of a few to dozens of clusters. Therefore the statistical uncertainty was large. Many authors also noted that cluster-to-cluster variation of the fraction of blue galaxies is considerable. The need for a larger, more uniform sample of clusters has been evident.

There have been various attempts to find another physical mechanism causing the large scatter which has been seen in almost all previous work. Wang & Ulmer (1997) claimed the existence of a correlation between the blue fraction and the ellipticity of the cluster X-ray emissions in their sample of clusters at $0.15 \leq z \leq 0.6$. Metevier, Romer & Ulmer (2000) showed that two clusters with a bimodal X-ray surface brightness profile have an unusually high blue fraction value and thus do not follow the typical Butcher-Oemler relation. They claimed that the Butcher-Oemler effect is an environmental phenomenon as well as an evolutionary phenomenon. Margoniner et al. (2001) found a richness dependence in the sense that richer clusters have smaller blue fractions. They claimed that this richness dependence causes a large scatter in the blue fraction–redshift diagram. Therefore, it is of extreme interest to explore an origin of the scatter in the blue fraction despite the redshift trend.

At the same time, various studies using morphological information have reported a similar evolution effect in cluster galaxies. Dressler et al. (1997) studied 10 clusters at $0.37 < z < 0.56$ and found a step increase in the S0 fraction toward *lower* redshift, compared to nearby clusters studied earlier (Dressler 1980). Couch et al. (1994,1998) studied three clusters at $z=0.31$ and found their S0 fraction to be consistent with the trend observed by Dressler et al. (1997). Fasano et al. (2000) observed nine clusters at intermediate redshifts ($0.09 < z < 0.26$) and also found an increase in the S0 fraction toward lower redshift. It has been proposed that the increase in the S0 fraction is caused by the transformation of spiral galaxies into S0 galaxies through a process yet unknown. These studies, however, need to be pursued further, considering that most of the previous work was based on morphological galaxy classification by eye. Although it is an excellent tool to classify galaxies, manual classification could potentially have unknown biases. (A detailed comparison of human classifiers can be found in Lahav et al. 1995). A machine based, automated classification would better control biases and would allow a reliable determination of the completeness and false positive rate. A further reason to investigate the evolution of cluster galaxies is the sample size. The morphological fraction studies of clusters reported so far are based on only dozens of clusters. Furthermore, the clusters themselves have intrinsic variety in the fraction of blue/spiral galaxies as reported by various Butcher-Oemler

and morphological analyses listed above. Since several authors have suggested that the fraction of blue galaxies depends on cluster richness, it is important to use a uniform cluster sample, preferably selected by an automated method with a well known selection function.

Various theoretical models have been proposed to explain the Butcher-Oemler effect and the increase of the S0 fraction. These models include ram pressure stripping of gas (Spitzer & Baade 1951, Gunn & Gott 1972, Farouki & Shapiro 1980; Kent 1981, Fujita 1998; Abadi, Moore & Bower 1999, Fujita & Nagashima 1999, Quilis, Moore & Bower 2000), galaxy infall (Bothun & Dressler 1986, Abraham et al. 1996a, Ellingson et al. 2001), galaxy harassment (Moore et al. 1996, 1999), cluster tidal forces (Byrd & Valtonen 1990, Valluri 1993), enhanced star formation (Dressler & Gunn 1992), and removal and consumption of the gas (Larson, Tinsley & Caldwell 1980, Balogh et al. 2001, Bekki et al. 2002). It is, however, yet unknown exactly what processes play major roles in changing the color and morphology of cluster galaxies. To derive a clear model explaining the evolution of cluster galaxies, it is important to clarify both the Butcher-Oemler effect and the S0 increase, using a large and uniform cluster sample in conjunction with a machine based morphological classification.

With the advent of the Sloan Digital Sky Survey (SDSS; York et al. 2000), which is an imaging and spectroscopic survey of 10,000 deg² of the sky, we now have the opportunity to overcome these limitations. The SDSS Cut & Enhance galaxy cluster catalog (Goto et al. 2002a) provides a large uniform cluster catalog with a well defined selection function. The CCD-based, accurate photometry of the SDSS (Fukugita et al. 1996, Hogg et al. 2002, Smith et al. 2002) and the wide coverage of the SDSS on the sky allow accurate estimation of blue fraction with robust local background subtraction. Although the SDSS is a ground based observation, the state-of-the-art reduction software and the accuracy of CCD data make it possible to derive morphological classification in an automated way (Lupton et al. 2001, 2002). By using the SDSS data set, we are able to study one of the largest samples to date — 514 clusters — to the depth of $M_r=-19.44$ ($h=0.75$).

The purpose of this paper is as follows. We aim to confirm or disprove the existence of the Butcher-Oemler effect using one of the largest, most uniform cluster samples. At the same time, we hope to shed light on the morphological properties of the Butcher-Oemler galaxies using morphological parameters derived from the SDSS data. Finally we investigate the origin of the scatter in the galaxy type fraction versus redshift relation, in hope of gaining some understanding about the physical processes responsible for the scatter.

Since several people reported that field galaxies also evolve both morphologically (Schade et al. 1996; Brinchmann et al. 1998; Lilly et al. 1998; Kajisawa et al. 2001; Abraham et al. 2001;) and spectroscopically (Madau et al. 1996; Lilly et al. 1996; Hammer et al. 1997; Treyer et al. 1998; Cowie et al. 1999; Sullivan et al. 2000; Wilson et al. 2002), it is of extreme importance to compare the evolution of cluster galaxies with that of field galaxies to specify a responsible physical mechanism. It is possible that the Butcher-Oemler effect and morphological transition

of cluster galaxies are more commonly happening including the field region of the universe, thus a cluster specific mechanism is not responsible for the evolution of galaxies. However, since the SDSS spectroscopic data are not deep enough to probe cosmologically interesting time scale, we leave it to future work.

The paper is organized as follows: In Section 2, we describe the SDSS data and the Cut & Enhance cluster catalog. In Section 3, we analyze the late type fraction, both spectrally and morphologically. In Section 4, we discuss the possible caveats and underlying physical processes in the evolution of galaxies. In Section 5, we summarize our work and findings. The cosmological parameters adopted throughout this paper are $H_0=75 \text{ km s}^{-1} \text{ Mpc}^{-1}$, and $(\Omega_m, \Omega_\Lambda, \Omega_k)=(0.3, 0.7, 0.0)$.

2. Data

The galaxy catalog used here is taken from the Sloan Digital Sky Survey (SDSS) Early Data Release (see Fukugita et al. 1996, Gunn et al. 1998, Lupton et al. 1999, 2001, 2002, York et al. 2000, Hogg et al. 2001, Pier et al. 2002, Stoughton et al. 2002 and Smith et al. 2002 for more detail of the SDSS data). We use equatorial scan data, a contiguous area of 250 deg^2 ($145.1 < \text{RA} < 236.0$, $-1.25 < \text{DEC} < +1.25$) and 150 deg^2 ($350.5 < \text{RA} < 56.51$, $-1.25 < \text{DEC} < +1.25$). The SDSS imaging survey observed the region to depths of 22.3, 23.3, 23.1, 22.3 and 20.8 in the u, g, r, i and z filters, respectively. (See Fukugita et al. 1996 for the SDSS filter system, Hogg et al. 2002 and Smith et al. 2002 for its calibration). Since the SDSS photometric system is not yet finalized, we refer to the SDSS photometry presented here as u^*, g^*, r^*, i^* and z^* . We correct the data for galactic extinction determined from the maps given by Schlegel, Finkbeiner & Davis (1998). We include galaxies to $r^*=21.5$ (petrosian magnitude), which is the star/galaxy separation limit (studied in detail by Scranton et al. 2002) in the SDSS data.

The galaxy cluster catalog used here is a subset of the SDSS Cut & Enhance galaxy cluster catalog (Goto et al. 2002a). There are 4638 clusters in the equatorial region (See Kim et al. 2002, Annis et al. 2002, Bahcall et al. 2002 and Miller et al. 2002 for other works on the SDSS galaxy clusters). Besides the uniformity of the catalog with its well defined selection function, the catalog has very good photometric redshifts, $\delta z=0.015$ at $z < 0.3$, which enables us to use a large sample of clusters (Goto et al. 2002a; see also Gal et al. 2000 and Annis et al. 2002 for photometric redshift methods for clusters). We use clusters in the redshift range of $0.02 \leq z \leq 0.3$ and galaxies brighter than $M_r = -19.44$, which corresponds to $r^*=21.5$ at $z=0.3$. Since several authors in previous work claimed that biases in sample cluster selection can mimic the evolutionary effect, it is important to control cluster richness well. We use clusters with more than 25 member galaxies between $M_{r^*} = -24.0$ and $M_r = -19.44$ within 0.7 Mpc after fore/background subtraction, as explained in the next Section. The large areal coverage of the SDSS data enables us to subtract the fore/background counts reliably. We can thus control the richness of the sample clusters well. The criteria leave 514 clusters in the region.

We stress the importance of the uniformity of the cluster catalog. Although the Abell cluster catalog (Abell 1958, Abell, Corwin and Olowin 1989) has been used in many studies, it was constructed by eye, and is sensitive to projection effects. When comparing clusters at different redshifts, it is particularly important to ensure that the data quality and cluster selection techniques are comparable, to avoid the introduction of potential selection biases. The SDSS Cut & Enhance cluster catalog used here is constructed using only the data taken with the SDSS telescope. Also, clusters are detected using a single algorithm (CE) throughout the entire redshift range ($0.02 \leq z \leq 0.3$). Combined with the well controlled richness criteria, our cluster sample is not only one of the biggest but also one of the most statistically uniform cluster catalogs. To study colors of galaxies in clusters, it is also important to use a cluster catalog created without targeting the red sequence of color magnitude relation of cluster galaxies. For example, Gladders & Yee(2000) and Annis et al. (2002) use a color filter targeting the red sequence of clusters and find galaxy clusters efficiently without suffering from projection effects. These techniques, however, can potentially have biases with regards to the colors of detected galaxy clusters, since clusters with a strong red sequence is more easily detected. They may not, therefore, be ideally suited to a Butcher-Oemler type of analysis. In contrast, the SDSS Cut & Enhance cluster catalog does not pick red galaxies selectively, and is therefore more suitable for this study. (Note that the the Cut & Enhance method does use generous color cuts. Although the color cut is designed to be wide enough to include blue galaxies in clusters, therefore it is not completely free from color originated biases.) In previous work, clusters have often been detected using data from only one or two color bands. This can introduce a bias, since higher redshift clusters are redder and fainter than lower redshift clusters. The SDSS Cut & Enhance cluster catalog detects clusters using four bands of the SDSS data (g, r, i and z), which minimizes the bias against redshift.

3. Analysis and Results

3.1. Fore/Background subtraction

We compute fractions of late-type galaxies in four different ways. First, we describe the statistical fore/background subtraction method we use. In counting galaxies, all galaxies are assumed to be at the cluster redshift to calculate absolute magnitudes. Then galaxies only between $M_{r^*} = -24.0$ and $M_{r^*} = -19.44$ are used in the analysis. We count the number of late-type/total galaxies within 0.7 Mpc from each cluster. Valotto et al. (2001) claimed that the global background correction can not correct background contamination appropriately. Following the claim, we use a local background correction. The number of late-type/total galaxies in fore/background is estimated using an annular area around each cluster with an inner radius of 2.1 Mpc and an outer radius of 2.21 Mpc in the same absolute magnitude range. The annulus fore/background subtraction enables us to estimate the fore/background locally,

minimizing variations in galaxy number counts due to the large scale structure. When an outer annulus touches the boundary of the region, a fore/background count is globally subtracted using galaxy number counts in the entire 400 deg² region by adjusting it to the angular area each cluster subtends. This fore/background subtraction is used in the analyses described in sections 3.2-3.5. The fraction of blue/late-type galaxies and its error are computed according to the following equations.

$$f_{late} = \frac{N_{c+f}^{late} - N_f^{late}}{N_{c+f}^{all} - N_f^{all}}, \quad (1)$$

$$\delta f_{late} = f_{late} \times \sqrt{\frac{N_{c+f}^{late} + N_f^{late}}{(N_{c+f}^{late} - N_f^{late})^2} + \frac{N_{c+f}^{all} + N_f^{all}}{(N_{c+f}^{all} - N_f^{all})^2} - \frac{2(\sqrt{N_f^{late} \times N_f^{all}} + \sqrt{N_{c+f}^{late} \times N_{c+f}^{all}})}{(N_{c+f}^{late} - N_f^{late})(N_{c+f}^{all} - N_f^{all})}} \quad (2)$$

where N_{c+f}^{late} and N_f^{late} represent numbers of blue/late-type galaxies in a cluster region and a field region, respectively. N_{c+f}^{all} and N_f^{all} represent numbers of all galaxies in a cluster region and a field region, respectively. The equation (2) assumes that N^{late} and N^{all} are not independent. We explain the derivation of equation (2) in Appendix 2.

3.2. Blue Fraction

The blue fraction of galaxy clusters (f_b) is measured as the fraction of galaxies bluer in $g-r$ rest frame color than the color of the ridge line of the cluster by 0.2 mag. This color criterion is equivalent to Butcher & Oemler's (1984) 0.2 mag in $B-V$ and Margoniner et al.'s (2000, 2001) 0.2 mag in $g-r$. The color of the ridge line is measured from the color-magnitude diagram using the same color-magnitude box used in measuring photometric redshift (Goto et al. 2002a). The colors of the ridge lines are confirmed to agree with empirical color of elliptical galaxies observed in the SDSS at the same redshift with less than 0.05 difference in $g-r$ color (Eisenstein, private communication). We also use Fukugita et al.'s (1995) model of an elliptical galaxy and a galaxy bluer than it by 0.2 mag in $g-r$. By redshifting these two galaxies, we measure $\delta(g-r)$ in the observed frame, which corresponds to the restframe $\delta(g-r)=0.2$. In calculating f_b , we count galaxies within 0.7 Mpc from the center of each cluster, which is the same radius as Margoniner et al. (2000, 2001), and corresponds to the average radius of Butcher & Oemler (1984). (We explore possible caveats in using fixed radius in Appendix.) Galaxies between $M_{r^*} = -24.0$ and $M_{r^*} = -19.44$ are counted, which corresponds to $r^*=21.5$ at $z=0.3$ for an average k -correction of all types of galaxies (Fukugita et al. 1995). Compared to the field luminosity function of Blanton et al. (2001), this includes galaxies as faint as $M_r^*+1.36$. Fore/background galaxies are statistically subtracted in the way described in Section 3.1. The lower left panel of Figure 1 shows f_b as a function of redshift. The error in f_b is estimated using equation (2) and the median values of the errors in f_b and z are shown in the upper left corner of the plot. Dashed line shows the weighted least-squares fit to the data. Solid lines and stars show the median values of the data. The scatter is considerable, but both of the lines show a clear increase of f_b toward higher redshift. The Spearman's correlation coefficient is 0.238 with

significance of more than 99.99% as shown in Table 1. The correlation is weak, but of high significance. The lower left panel of Figure 2 further clarifies the evolution effect. A dashed and a solid line show normalized distributions of f_b for clusters with $z \leq 0.15$ and $0.15 < z \leq 0.3$, respectively. The two distributions are significantly different at the 98% level, as determined by a Kolomogorov-Smirnov test. The slope shown with the dashed line rises up to $f_b \sim 0.2$ at $z=0.3$ (look back time of ~ 3.5 Gyr), which is consistent with previous work such as Butcher & Oemler (1978,1984), Rakos & Schombert (1995), Margoniner et al. (2000, 2001), within the scatter. We conclude that the Butcher-Oemler effect is seen in the SDSS Cut & Enhance galaxy cluster catalog.

We caution readers on the systematic uncertainties in measuring f_b . Marzke et al.(1994,1997,1998), Lin et al. (1999) and Blanton et al. (2001) showed that luminosity functions of galaxy clusters depend significantly on galaxy type, in such a way that the bright end of the cluster luminosity function is dominated by redder galaxies and the faint end is dominated by bluer galaxies. Boyce et al.(2001) and Goto et al. (2002b) showed that a similar tendency exists for cluster luminosity functions. This difference in luminosity functions leads to a different blue fraction depending on the absolute magnitude range used. Furthermore, if the radial distributions of blue and red galaxies are different (*e.g.* Kodama et al. 2001), the f_b measurement depends heavily on the radius. When comparing with previous work, therefore, it is important to take account of the exact method used to calculate f_b . We discuss the uncertainty in measuring blue fractions further in Section 4.

3.3. Late Type Fraction Using $u - r < 2.2$

Recently Shimasaku et al. (2001) and Strateva et al. (2001) showed that the SDSS $u - r$ color correlates well with galaxy morphologies. In this section we use $u - r$ color to separate early($u - r \geq 2.2$) and late ($u - r < 2.2$) type galaxies as proposed by Strateva et al. (2001). Note that although $u - r$ color is claimed to correlate well with galaxy types, it is still a color classifier and thus different from the morphological parameters we investigate in the following two sections. The methodology used to measure late type fraction is similar to the one we use to measure f_b . We regard every galaxy with $u - r < 2.2$ as a late type galaxy. We define f_{u-r} as the ratio of the number of late type galaxies to the total number of galaxies within 0.7 Mpc. Fore/background subtraction is performed in a way described in Section 3.1. The upper left panel of figure 1 shows f_{u-r} as a function of redshift. The error in f_{u-r} is calculated using equation (2) and the median values of the errors in f_{u-r} and z are shown in the upper left corner of the panel. The dashed line shows the least square fit to the data. The solid lines and stars show the median values of the data. As in the case of f_b , the scatter is considerable, but the weak increase of the late type galaxies is seen. The Spearman's correlation coefficient is 0.234 and is inconsistent with zero at greater than 99.99% confidence level (Table 1). Again, weak but significant correlation is found. The upper left panel of Figure 2 shows distributions

of f_{u-r} for $z \leq 0.15$ clusters and $0.15 < z \leq 0.3$ clusters with a dashed and solid line, respectively. A Kolomogorov-Smirnov test shows that the distributions are different with more than a 99% significance. In addition to the increase in f_b shown in the last Section, the increase in f_{u-r} provides further evidence of color evolution of cluster galaxies. Furthermore, since $u-r$ color of galaxies is sensitive to a galaxy's morphology as shown in Figure 6 of Strateva et al (2001), it suggests possible evolution of morphological types of galaxies as well. We investigate the morphological evolution of galaxies in clusters in the next subsection.

3.4. Late Type Fraction Using Profile fitting

One of the purposes of this paper is to determine if there is a morphological change of galaxies in clusters as a function of redshift. The SDSS photometric pipeline (PHOTO; Lupton et al. 2002) fits a de Vaucouleur profile and an exponential profile to every object detected in the SDSS imaging data and returns the likelihood of the fit. By comparing the likelihoods of having an exponential profile against that of a de Vaucouleur profile, we can classify galaxies into late and early types. In this section, we regard every galaxy that has an exponential likelihood higher than a de Vaucouleur likelihood in r band as a late type galaxy. A galaxy with higher de Vaucouleur likelihood in r band is regarded as an early type galaxy. We define f_{exp} in the same way as in previous subsections. *i.e.* f_{exp} is the ratio of the number of late type galaxies to the total number of galaxies within 0.7 Mpc. Fore/background counts are corrected using the method described in Section 3.1. The resulting f_{exp} is plotted in the lower right panel of Figure 1. The error in f_{exp} is estimated using equation (2) and the median values of the errors in f_{exp} and z are shown in the upper left corner of the plot. The dashed line shows the weighted least-squares fit. The solid lines and stars show the median values of the data. The scatter is considerable, but we see the increase of f_{exp} toward the higher redshift. The Spearman's correlation coefficient is 0.194, which is inconsistent with zero at more than a 99.99% confidence level (Table 1). The upper right panel of Figure 2 shows the distributions of clusters with $z \leq 0.15$ and with $0.15 < z \leq 0.3$ with a dashed and solid line, respectively. The two distributions show a difference of more than 99% significance in a Kolomogorov-Smirnov test. We emphasize that the galaxy classification used here is purely morphological — independent of colors of galaxies. The fact that we still see the increase of the late type galaxies toward higher redshift suggests that these Butcher-Oemler type blue galaxies also change their morphological appearance as well as their colors. We also point out that the slope of the change is similar to the panel in the lower left of Figure 1, which is $\sim 30\%$ between $z=0.02$ and $z=0.3$. We note that there is a potential bias associated with the use of r band profile fitting throughout the redshift range, since the r band wavelength range at $z=0.3$ is almost that of g band at restframe. We investigate this effect in Section 4, and conclude that it is small. Like the blue fraction, the morphological late-type fraction is also sensitive to the magnitude range considered. Binggeli et al. (1988), Loveday et al. (1992), Yagi et al. (2002a,b) and Goto et al. (2002b) reported

luminosity functions of elliptical galaxies have brighter characteristic magnitudes and flatter faint end tails compared to those of spiral galaxies in both field and cluster regions. Careful attention should be paid to the magnitude range used in an analysis when fractions of spiral galaxies are compared. We discuss the uncertainty further in Section 4.

3.5. Late Type Fraction Using Concentration Parameter

As another morphological galaxy classification method, we use the inverse of the concentration parameter (C_{in}) advocated by Shimasaku et al. (2001) and Strateva et al. (2001). We define C_{in} as the ratio of Petrosian 50% radius to Petrosian 90% radius in r band. They are the radii which contain 50% and 90% of Petrosian flux, respectively. (See Stoughton et al. 2002 for more details of Petrosian parameters). Since C_{in} is the inverse of a conventional concentration parameter, spiral galaxies have a higher value of C_{in} . Following Strateva et al. (2001), we use $C_{in}=0.4$ to divide galaxies into early and late type galaxies. Readers are referred to Morgan (1958,1959), Doi, Fukugita & Okamura (1993) and Abraham et al. (1994, 1996) for previous usage of concentration of light as a classification parameter. $f_{C_{in}}$ is defined as the ratio of the number of galaxies with $C_{in} > 0.4$ to the total number of galaxies within 0.7 Mpc as in the previous subsections. Note that our early type galaxies with $C_{in} < 0.4$ include S0 galaxies in addition to elliptical galaxies since discerning elliptical and S0 galaxies is very difficult with the SDSS data, in which the seeing is typically $1.5''$. (See Shimasaku et al. 2001 and Strateva et al. 2001 for the correlation of C_{in} with an eye classified morphology). Fore/background number counts are corrected as described in Section 3.1. The absolute magnitude range used is $-24 < M_r < -19.44$. The upper right panel of Figure 1 shows $f_{C_{in}}$ as a function of redshift. Since the classification using $C_{in}=0.4$ leans toward late type galaxies, the overall fraction is higher than the other panels in the figure. The increase of late type fraction, however, is clearly seen. The dashed line shows the weighted least-squares fit. The solid lines and stars show the median values of the data. The error in $f_{C_{in}}$ is estimated using equation (2) and the median values of the errors in $f_{C_{in}}$ and z are shown in the upper left corner of the plot. The Spearman's correlation coefficient is 0.223 with significance of more than 99.99% as shown in Table 1. The upper right panel of Figure 2 further clarifies the evolution effect. The distribution of $z \leq 0.15$ clusters in a dashed line and the distribution of $0.15 < z \leq 0.3$ clusters in a solid line show a difference with more than a 99% significance level. We stress that the galaxy classification based on this concentration parameter is purely a morphological one. In this morphological classification, we still see the increase of the late type fraction just like the increase of f_b — as if observing the morphological equivalence of the Butcher-Oemler effect. The increase in $f_{C_{in}}$ combined with the increase in f_{exp} provides rather firm evidence of morphological change in the Butcher-Oemler type galaxies. Possible caveats in the usage of C_{in} and comparisons with previous works are discussed in Section 4.

3.6. On the Origin of the Scatter

In the last four sections, we observed the increase of late type fractions toward higher redshift in all the four cases. At the same time, we see a significant amount of scatter around the late type fraction v.s. redshift relations. Although the errors on these measurements are also large, this scatter might suggest that there might be one or more physical properties which determine the amount of late-type galaxies in clusters. Table 3 compares median error sizes of f_b , f_{u-r} , f_{exp} and f_{Cin} with scatters around the best-fit lines (dotted lines in Figure 1). In fact, in all cases, real scatters are larger than the statistical errors. In the literature, several correlations are proposed such as with X-ray shapes of clusters (Wang et al. 2001, Metevier et al. 2000), and cluster richness (Margoniner et al. 2000). Our cluster richnesses are plotted against redshift in Figure 3. Richnesses are measured as numbers of galaxies between $M_r = -24.0$ and $M_r = -19.44$ within 0.7 Mpc after fore/background subtraction, as explained in Section 3.1. In figure 3, this richness has no apparent bias with redshift. In Figure 4, the difference of the late type fraction from the best-fit line is plotted against cluster richness. The circles and solid lines show median values. In all the panels, there is a clear tendency of richer clusters having a lower fraction of late type galaxies. This tendency is in agreement with Margoniner et al. (2000) who found richer clusters had lower blue fractions. We further discuss the richness dependence of the late type fraction in Section 4 and Appendix. As an alternative parameter to X-ray shape, we plot the difference from the best-fit line against cluster elongation in Figure 5. The elongation parameter is taken from Goto et al. (2002a), which measured the ratio of major and minor axes in their enhanced map to find clusters. Circles and solid lines show median values. No obvious trend is seen here. Our result seems to agree with Smail et al.'s (1997) caution that a correlation between f_b and cluster ellipticity found by Wang et al. (1997) could be due to a small and diverse sample. However, since distribution of galaxy positions might not represent cluster ellipticities well, we do not conclude that there is no dependence on cluster ellipticities. The dependence should be pursued further in the future, ideally using X-ray profile shape with a large sample of clusters.

4. Discussion

4.1. Morphological k -correction

In the upper right panel of Figure 1, we use C_{in} (inverse of concentration index) in the r band to classify galaxies throughout our redshift range ($0.02 \leq z \leq 0.3$). This could potentially cause redshift dependent biases in our calculation of C_{in} . Since the universe is expanding, by analyzing the observed r band data, we are analyzing bluer restframe wavelengths in the higher redshift galaxies. In fact, the r band at $z=0.3$ is almost g band in the restframe. Various authors have pointed out that galaxy morphology significantly changes according to the wavelength used (*e.g.* Abraham et al. 2001). To estimate how large this bias is, we plot the

normalized distributions of C_{in} in g and r bands in Figure 6 using the galaxies with $0.02 \leq z \leq 0.03$ in the SDSS spectroscopic data (1336 galaxies in total; See Eisenstein et al. 2001, Strauss et al. 2002 and Blanton et al. 2002 for the SDSS spectroscopic data). In this redshift range, the color shift due to the expansion of the universe is small. We use this to study the dependence of the C_{in} parameter on the restframe wavelength. At $z=0.3$, r band corresponds to restframe g band. The solid and dashed lines show the distribution for g and r bands, respectively. The two distributions are not exactly the same, but the difference between the two distributions is small. We summarize the statistics in Table 4. There are 802/1336 galaxies with $C_{in} > 0.4$ in g band, and 787/1336 galaxies have $C_{in} > 0.4$ in r band. The difference is 15/1336 galaxies, which is 1.1% of the sample. In section 3.5, the change in $f_{C_{in}}$ is $\sim 30\%$. The effect of the morphological k-correction is therefore much smaller. We also point out that this analysis assumes the largest difference in redshift ($0.02 \leq z \leq 0.3$), therefore it gives the upper limit of the bias. Since the majority of our clusters are at $z \sim 0.2$, the wavelength difference between the observed and restframe bands is typically much smaller. We conclude that the effect of the morphological k-correction is much smaller than the change in $f_{C_{in}}$ we observed in Section 3.5.

In Section 3.4, we use the r band fit for all galaxies in our sample. The same redshift effect could potentially bring bias to our analysis. In Table 5, we limit our galaxies to $0.02 \leq z \leq 0.03$ and count the fraction of late type galaxies in the g and r bands corresponding to observed frame r band at $z=0.0$ and $z=0.3$. We list the number of galaxies with exponential likelihood higher than de Vaucouleur likelihood in column 1, the total number of galaxies in column 2, and the ratio of columns 1 to 2 in column 3. As shown in the 3rd row, the difference in the fraction of late type galaxies between g band data and r band data is only 2.5%, which is much smaller than the f_{exp} change we see in the upper right panel of Figure 1 ($\sim 30\%$). We conclude that the change of f_{exp} and $f_{C_{in}}$ is not caused by the small redshift bias in using r band data throughout the redshift range.

4.2. Seeing Dependence

Another possible source of bias in measuring f_{exp} and $f_{C_{in}}$ is the dependence on the seeing, relative to the size of the galaxies. At higher redshift, the size of a galaxy is smaller and a seeing convolution could be more problematic. Especially for the concentration parameter (C_{in}), galaxy light becomes less concentrated when the seeing size is comparable to the galaxy size, and thus, the effect could cause a bias towards higher C_{in} values. To check this, we plot $f_{C_{in}}$ against the point-spread function (PSF) size in the r band for two redshift limited samples in Figure 7. Open squares and solid lines show the distribution and medians of low z clusters ($z \leq 0.15$). Filled triangles and dashed lines show the distributions and medians of high z clusters ($0.24 < z \leq 0.3$). For the median measurements, bins are chosen so that equal numbers of galaxies are included in each bin. 1σ errors are shown as vertical bars. As expected, lower redshift clusters show almost negligible dependence on seeing size. Higher redshift clusters show about

a 5% increase in f_{Cin} between the best and worst seeing size. The evolution effect we see in the upper right panel of Figure 1 is more than 20%. Furthermore, as the distribution of seeing in Figure 8 shows, 87% of our sample galaxies have seeing better than $2.0''$. Therefore we conclude that varying seeing causes a small bias which is significantly weaker than the evolution we find in Section 3. The effect of varying seeing is less significant for the f_{exp} parameter. In Figure 9, we plot f_{exp} against seeing size for two redshift samples with redshift ranges and symbols as in Figure 7. 1σ errors, shown as vertical bars, are dominant. There is no significant correlation of f_{exp} with seeing size.

4.3. Radius, Fore/background Subtraction and Cluster Centroids

Throughout the analyses in Section 3, we use a 2.1-2.21 Mpc annular region for fore/background subtraction. In return for taking cosmic variance into account, annular (local) background subtraction has larger errors than global background subtraction due to its smaller angular area coverage. However the difference is not so large. In case of blue galaxy counts (f_b) in the background, the median Poisson (1σ) uncertainty for global background is 12.2%, whereas 1σ variation of local background is 12.6%. This increases the errors, but only by 0.4 points. The actual effect to the late-type fraction is plotted in Figure 10. Solid lines show distributions for our default choice of 0.7 Mpc radii and 2.1-2.21 Mpc annuli. Dashed lines show distributions for global fore/background subtraction, where fore/background subtraction is performed using global number counts of galaxies for all the clusters in the sample. A Kolomogorov-Smirnov test between two samples does not show any significant difference.

For cluster radius, we use 0.7 Mpc, since we do not have information about the virial radii of each system. It is, however, ideal to use virial radii since, for example, in a standard cold dark matter cosmology, virial radii at a fixed mass scales as $\propto (1+z)^{-1}$. Another possible cause of uncertainty is the accuracy in deciding cluster centers. In this work, a center position of each cluster is taken from Goto et al. (2002a), and is estimated from the position of the peak in their enhanced density map. Although, from Monte-Carlo simulations, cluster centroids are expected to be determined with an accuracy better than ~ 40 arcsec, the offsets have a possibility to introduce a bias in our analyses. We test different choices of these parameters in Figure 10. Dotted lines show distributions where radii change as $0.7 \times (1+z)^{-1}$ Mpc assuming a standard cold dark matter cosmology. Long dashed lines show distributions when the position of brightest cluster galaxy (within 0.7 Mpc and $Mr < -24.0$) is used as a cluster center. Kolomogorov-Smirnov tests show no significant difference in any of the above cases. In all cases, the probability that the distributions are different is less than 26%. Our results in Section 3 are thus not particularly sensitive to our choice of annuli, radii or cluster centers. We further pursue the effect of radius dependence of blue/late type fractions in Appendix, and show that it does not change our main results.

4.4. Comparison with Late-type Fraction from Spectroscopy

To further test our late-type fraction measurement, we compare the late-type fraction obtained from the SDSS spectroscopic data with that obtained from the SDSS imaging data in figure 11. Since the SDSS spectroscopic data are limited to $r^* < 17.77$ (Strauss et al. 2002), the comparison can be done only for clusters with $z < 0.06$. In the literature, three clusters are found to satisfy these criteria in the region used in this study. The clusters include ABELL 295, RXC J0114.9+0024, and ABELL 957. For these clusters, late-type fractions are measured in the same way as in section 3. Late-type fractions from spectroscopy are measured using galaxies within 0.7 Mpc and $\delta z = \pm 0.005$ from the redshift of each cluster. Note that there is no fore/background correction for spectroscopic late-type fraction. In figure 11, all points agree with each other within the error. The good agreement suggests that our fore/background subtraction technique described in section 3.1 works properly. It would be ideal to perform the same test for high redshift clusters as well. However, the SDSS spectroscopic data are not deep enough to perform the test for higher redshift clusters.

4.5. The Butcher-Oemler Effect

The Butcher-Oemler effect— an increase in the ratio of blue galaxies in clusters as a function of redshift— is strong evidence of direct evolution of the stellar populations in galaxies; it has been studied by numerous authors in the past. In this section, we compare our results with previous work. Since different authors use different cluster samples, color bands, cosmology, absolute magnitude ranges and methods of fore/background subtraction, which could affect the comparison, we emphasize the differences in analysis by each author. Note that one important difference is that some previous work used a sample of quite rich clusters. e.g. clusters with more than 100 members in magnitude and radius ranges comparable to those adopted in this study. Poorest systems in our sample have only 25 member galaxies after fore/background subtraction. Thus, difference in cluster samples could cause a difference in results.

Butcher & Oemler (1978, 1984) studied 33 clusters between $z=0.003$ and $z=0.54$. They used galaxies brighter than $M_V = -20$ ($h=0.5$ and $q_0=0.1$) within the circular area containing the inner 30% of the total cluster population. They found f_b increases with redshift for $z \geq 0.1$. Their f_b at $z=0.3$ is ~ 0.15 , which is slightly lower than our value. Considering the large scatter in both their and our samples, we do not claim that our results are inconsistent with their value. Note that Andreon & Ettori (1999) found a trend of increasing X-ray luminosity with increasing redshift in the sample clusters of Butcher & Oemler (1984).

Rakos & Schombert (1995) studied 17 clusters using Stromgren *uvby* filters. Due to the usage of the narrow band filters redshifted to the cluster distance, their study did need to use model-dependent k-corrections. However, their high-redshift cluster sample is drawn from that of Gunn, Hoessel & Oke (1986) which is based on IIIa-J and IIIa-F photographic plates. At $z > 0.5$, these plates measure the rest-frame ultraviolet to blue region of the spectrum. Thus

the cluster catalog will be biased toward clusters rich in blue galaxies at high redshift. Rakos & Schombert found $f_b \sim 0.25$ at $z=0.3$, which is slightly higher than the estimation of Butcher & Oemler (1984) but in agreement with our results.

Margoniner et al. (2000) studied 44 Abell clusters between $z=0.03$ and $z=0.38$. They used galaxies between $M_r = -21.91$ and $M_r = -17.91$ ($h = 0.75$) within 0.7 Mpc of the cluster center. The fore/background counts are subtracted using five control fields. Their results are more consistent with the steeper relation estimated in 1995 by Rakos and Schombert than with the original one by Butcher and Oemler in 1984. The results are also consistent with ours. Margoniner et al. (2001) extended their work to 295 Abell clusters and found $f_b = (1.34 \pm 0.11) \times z - 0.03$ with a *r.m.s.* of 0.07, which is in agreement with our fitted function shown in Figure 1.

Ellingson et al. (2001) studied 15 CNOC1 clusters (Yee, Ellingson, & Carlberg 1996) between $z=0.18$ and $z=0.55$. Since they used spectroscopically observed galaxies, they do not suffer from the fore/background correction (but see Diaferio et al. 2001). They used galaxies brighter than $M_r = -19.0$ within r_{200} from the cluster center (with an average of $1.17h^{-1}$ Mpc). Their best fit shows $f_b \sim 0.15$ at $z=0.3$. The scatter in their Fig. 1 and our data are both substantial. Thus, we can not conclude this is inconsistent with our results.

All of these authors found considerable scatter in f_b v.s. z plot as is seen in our Figure 1. It is promising that our results are consistent with the previous work within the scatter, despite the differences in the radial coverage and magnitude ranges used.

4.6. Morphological Butcher-Oemler effect

In sections 3.3, 3.4, and 3.5, we found an increase in the fraction of late type galaxies selected by morphological parameters with increasing redshift — as if the Butcher-Oemler effect is happening morphologically. Perhaps revealing this morphological Butcher-Oemler effect is the most striking result of this study. It suggests that the Butcher-Oemler blue galaxies change their morphology from late to early type at the same time that they change their color from blue to red. Although accurately quantifying the fraction of galaxies which experience the morphological Butcher-Oemler effect is difficult due to the considerable scatter in the data, our best-fit lines suggest that $\sim 30\%$ of galaxies in clusters go through this transition between $z=0.3$ and $z=0.02$.

In previous work, Dressler et al. (1997) found a deficit of S0 galaxies in 10 intermediate ($z \sim 0.5$) clusters by classifying galaxy morphology in the HST image by eye. They claimed that many S0s needed to be added to reach the fraction of S0s found in present clusters (Dressler 1980). Couch et al. (1994, 1998) also found an indication of morphological transformation in the Butcher-Oemler galaxies by studying three rich clusters at $z=0.31$. Later, Fasano et al. (2000) showed that spiral galaxies are, in fact, turning into S0 galaxies by observing nine clusters at intermediate redshifts and analyzing them together with higher redshift clusters in

the literature. Their galaxy morphology was also based on eye classification. Our SDSS data is taken using ground based telescopes with moderate seeing ($\sim 1.5''$), and thus does not allow us to separate S0 galaxies from elliptical galaxies as the HST does. The advantage of our classification is its automated nature, which allows accurate reproducibility and quantification of systematic biases. In particular, it is easy to compute the completeness and contamination rate for the automated classification, based on simulations; for the present sample, the completeness and contamination rate of the parameters are given in Shimasaku et al. (2001) and Strateva et al. (2001). Furthermore, an automated galaxy classification is easier to reproduce in future observational work and in detailed computer simulations. Although we can not distinguish S0s from ellipticals, the increase of blue fraction and increase of late type galaxies toward higher redshift is qualitatively consistent with the process of S0 production over the interval in cosmic time suggested by previous investigations.

Various physical mechanisms could be the cause of the morphological and spectral Butcher-Oemler effects. Possible causes include ram pressure stripping of gas (Gunn & Gott 1972, Farouki & Shapiro 1980; Kent 1981, Abadi, Moore & Bower 1999, Quilis, Moore & Bower 2000), galaxy infall (Bothun & Dressler 1986, Abraham et al. 1996a, Ellingson et al. 2001), galaxy harassment via high speed impulsive encounters (Moore et al. 1996, 1999), cluster tidal forces (Byrd & Valtonen 1990, Valluri 1993) which distort galaxies as they come close to the center, interaction/merging of galaxies (Icke 1985, Lavery & Henry 1988, Bekki 1998), and removal & consumption of the gas due to the cluster environment (Larson, Tinsley & Caldwell 1980, Balogh et al. 2001, Bekki et al. 2002). Mamon (1992) and Makino & Hut (1997) showed that interactions/mergers can occur in a rich cluster environment despite the high relative velocities. Shioya et al. (2002) showed that the truncation of star formation can explain the decrease of S0 with increasing redshift. It has been known that preheating of intergalactic medium can effect morphologies of galaxies by strangling the gas accretion (Mo & Mao 2002; Oh & Benson 2002). In fact, Finoguenov et al. (2003) found the filamentary gas in Coma cluster and predicted quiescent star formation in galaxy disks around the filament. Although our results provide some important clues, pinpointing what processes are responsible in the morphological and spectral Butcher-Oemler effect is a more difficult challenge.

Our results suggest that the cause will be one that affects both color and morphological appearance of galaxies at the same time. Couch et al. (1998), Dressler et al. (1999) and Poggianti et al. (1999) found “passive spirals”, which are galaxies with spiral morphology but without star formation. They are probably belong to the same population as “anemic spirals” found by van den Bergh (1976). The mechanism creating “passive spirals” or “anemic spirals”, however, affects only the color of galaxies and, thus, probably is not the main mechanism that accounts for the entire effect. The increase of morphologically late type galaxies toward higher redshifts at the same time as the increase of blue galaxies is consistent with mechanisms which affect the gas supply (e.g. ram-pressure stripping, galaxy infall). However if the infalling rate

of field galaxies (mostly blue/late type) is higher in the past, almost any of the mechanisms mentioned above can explain our observational results. Furthermore, although we discussed about cluster specific phenomena, it is also known that galaxies in the field region evolve as a function of redshift as well. (e.g. Hammmer et al. 1996; Lilly et al. 1996; Balogh et al. 1997, 2002). The evolution of field galaxies needs to be compared with that of cluster galaxies further in detail. Therefore, it is still an open question what mechanism causes spectral and morphological evolution of cluster galaxies.

The finding of a 30% change of the fraction during the look back time of ~ 3.5 Gyr could also give us an additional hint in finding an underlying physical process. If the gas in spiral galaxies is removed very efficiently by some physical processes (e.g. ram-pressure stripping) or consumed rapidly by star formation, the spiral arms will disappear after several disk rotation periods, ~ 1 Gyr (Sellwood & Carlberg 1984). Interaction/merger processes are quicker than gas removal processes (~ 0.5 Gyr; Mihos 1995). Moore et al.'s (1996) simulation showed that the galaxy harassment phase lasts for several Gyr. Kodama et al. (2001) used the phenomenological simulations to show that the timescale of the morphological transformation from spiral to S0 is $1\sim 3$ Gyr. For spectral change, Shioya et al. (2002) showed that a disk needs 2-3 Gyr after the removal of gas (or truncation of star formation) to show a k spectrum. Poggianti et al. (1999) compared the spectral and morphological properties of cluster galaxies and suggested that the timescale of the morphological transition is longer than that of the spectral transition. This difference in timescale is interesting since if one process is significantly quicker than the other, we might be able to see the time difference in the decreases in the fraction of late type galaxies and blue galaxies, which will provide a strong constraint in the evolution history of the Butcher-Oemler galaxies. In Figure 1, we see a $\sim 30\%$ of change in both the photometric and morphological Butcher-Oemler effect between $z=0.02$ and $z=0.30$ (~ 3.5 Gyr). The scatter in our measurement, however, is considerable and our choices of criteria between late and early type galaxies do not necessarily coincide with each other. It is thus not straightforward to convert the information to the time scale of the responsible physical process. In addition, to understand change in fraction of morphological and spectral late-type galaxies, the change in infalling rate of field galaxies needs to be understood as well. Since computer simulations have recently made dramatic progress, in the near future it will become possible for state-of-the-art simulations to simulate both dynamical and spectral evolutions of cluster galaxies, plus infalling rate of field galaxies in order to compare the results with the observed trend. For example, such a simulation can be done by combining dynamical simulations (e.g. Evrard 1991, Kauffmann et al. 1995, Bekki, Shioya & Couch 2001, Vollmer et al. 2001, Bekki et al. 2002) with cluster phenomenological simulations (e.g. Abraham et al. 1996, Fujita 1998,2001, Balogh et al. 1999, Stevens, Acreman, & Ponman 1999, Balogh, Navarro, & Morris 2000, Kodama & Bower 2001). Figure 1 in this work provides the interesting observational data to tackle with using such a simulation of cluster galaxy formation.

4.7. Richness Dependence

In Section 3.6, we observe the tendency of richer clusters to have smaller fractions of late type galaxies, by measuring the residuals from the best fit relations as a function of cluster richness. Our result is consistent with Margoniner et al. (2001), who used a similar optical richness to find that poorer clusters tend to have larger blue fractions than richer clusters at the same redshift. Figure 4, however, still shows a significant amount of scatter, which might be suggesting the existence of another factor in determining the blue fraction in addition to redshift and richness. The dependence of the late type fraction on cluster richness, however, provides another hint on the underlying physical processes. Since ram pressure is stronger in clusters with higher temperature at the same gas density, Fujita & Nagashima(1999) theoretically predicted that if ram pressure is the only mechanism responsible for the evolution of galaxies in clusters, the fraction of blue galaxies will always be higher in lower X-ray luminosity clusters, which usually have low temperatures. Our data shown in Figure 4 are consistent with the prediction from their ram pressure stripping model. Although our richness is from numbers of galaxies in optical imaging data, it is reasonable to assume it correlates well with X-ray luminosity (Bahcall 1977; Bower et al. 1994). Then, the optical richness can be related to the gas temperature through the well known $L_X - T$ relation (Mitchell, Ives, and Culhane 1977; Henry & Arnaud 1991; Edge & Stewart 1991; David et al. 1993; White, Jones, and Forman 1997; Allen & Fabian 1998; Markevitch 1998; Arnaud & Evrard 1999; Jones & Forman 1999; Reichart, Castander, & Nichol 1999; Wu, Xue, and Fang 1999; Xue & Wu 2000; and see the references therein). In a simple estimation, ram pressure is proportional to ρv^2 . L_X is proportional to ρ^2 . From the virial theorem, $v^2 \propto T$. The $L_X - T$ relation studied by Xue & Wu (2000) is $L_X \propto T^{2.8}$. Therefore, ram pressure is proportional to $\sim L_X^{0.86}$. Combined with an assumption that optical richness scales with X-ray luminosity (see, e.g. Bahcall 1974, Jones & Forman 1978, Bower et al. 1994, and Miller et al. in preparation), Figure 4 provides another hint that ram pressure stripping induces the evolution of cluster galaxies.

In the literature, however, the dependence of blue fractions on cluster richness has been controversial. Bahcall (1977) studied 14 X-ray clusters and found that the fraction of spiral galaxies decreases with increasing X-ray luminosity. Lea & Henry(1988) observed 14 clusters in X-ray and found that the percentage of blue objects in the clusters seems to increase with the X-ray luminosity. On the other hand, Fairley et al. (2002) studied eight X-ray selected clusters and did not find any dependence of blue fractions on X-ray luminosities. Balogh et al. (2002) studied 10 clusters at $z=0.25$ with low X-ray luminosity and found similar morphological and spectral properties of galaxies compared with clusters with high X-ray luminosity (Balogh et al. 1997). In all cases, the results were based on a small sample of clusters. We also point out that although our results are consistent with a ram-pressure stripping model, there is a possibility that the other mechanisms could explain the phenomena. For example, richer clusters might have higher rate of merger/interaction due to their higher galaxy density. The same argument

holds true for galaxy harassment. Thus, more study is needed to conclude about the physical mechanism causing the phenomena. In the near future, confirming the richness dependence using X-ray luminosities or velocity dispersions with a larger sample of clusters would offer us more insight on the subject.

5. Conclusions

In this paper, we have investigated the fraction of late type galaxies in four different ways using one of the largest, most uniform samples of 514 clusters between $0.02 \leq z \leq 0.3$ from the SDSS Cut & Enhance galaxy cluster catalog. All the clusters selected here have more than 25 member galaxies within 0.7 Mpc and between $M_r = -24.0$ and $M_r = -19.44$ after statistical local fore/background subtraction. The following four different ways to estimate the fractions of late type galaxies are adopted: restframe $g - r$ color (a classical Butcher-Oemler estimator), $u - r$ color, concentration index and de Vaucouleur/exponential profile fit. The last three parameters are known to correlate well with galaxy morphologies (Shimasaku et al. 2001, Strateva et al. 2001). In all four cases, we observe an increase of the fraction of late type galaxies toward higher redshift with a significance of more than 99.99% (Table 1). We draw the following conclusion from this work.

1. We confirm the presence of the Butcher-Oemler effect using $g - r$ color. The Butcher-Oemler effect is real and exists in our sample clusters as seen in the lower left panel of Figure 1. The slope of the increase is consistent with previous work although the scatter in the blue fraction is considerable. Previous work also noted a large scatter in the fraction of blue galaxies. The fraction of late type galaxies also shows a similar increase when we use a $u - r$ color cut.

2. We observe a morphological Butcher-Oemler effect as an increase of late type galaxies toward higher redshift, using pure morphological parameters such as a concentration parameter and de Vaucouleur/exponential profile fit. The rates of increase are consistent with previous work on the spiral to S0 transition, albeit with considerable scatter (Figure 1). The increase is also in agreement with the original Butcher-Oemler effect from $g - r$ color. Our results are consistent with the evolutionary scenario proposed by Dressler et al. (1997), Smail et al. (1997), Couch et al. (1998), and Kodama & Smail (2002), in which there is a progressive morphological conversion in clusters from spirals into E/S0's.

3. We find a slight tendency for richer clusters to have lower values of the late type fraction (Figure 4). This trend agrees with the ram pressure stripping model proposed by Bahcall (1977) and Fujita et al. (1999), in which galaxies in richer clusters are more affected by ram pressure due to their high temperature.

Although our results 1,2, and 3 are all consistent with a ram-pressure stripping model, there still remains a possibility that other physical mechanisms are responsible for the evolution of cluster galaxies. Thus, further study is needed both theoretically and observationally to reveal the underlying physical mechanism responsible for the evolution of cluster galaxies. Since this

work is based on only 5% of the whole SDSS data, an increase in the data will improve the statistical accuracy as the SDSS proceeds. Extending the work to higher redshifts using 4-8 m class telescopes will offer more insight on the origin and evolution of cluster galaxies.

We are grateful to Nell Hana Hoffman, Ricardo Colon, Michael L. Balogh, A. Kathy Romer and Robert C. Nichol for valuable comments, which contributed to improve the paper. We thank anonymous referee for valuable comments, which improved the paper significantly. T.G. acknowledges financial support from the Japan Society for the Promotion of Science (JSPS) through JSPS Research Fellowships for Young Scientists.

Funding for the creation and distribution of the SDSS Archive has been provided by the Alfred P. Sloan Foundation, the Participating Institutions, the National Aeronautics and Space Administration, the National Science Foundation, the U.S. Department of Energy, the Japanese Monbukagakusho, and the Max Planck Society. The SDSS Web site is <http://www.sdss.org/>.

The SDSS is managed by the Astrophysical Research Consortium (ARC) for the Participating Institutions. The Participating Institutions are The University of Chicago, Fermilab, the Institute for Advanced Study, the Japan Participation Group, The Johns Hopkins University, Los Alamos National Laboratory, the Max-Planck-Institute for Astronomy (MPIA), the Max-Planck-Institute for Astrophysics (MPA), New Mexico State University, Princeton University, the United States Naval Observatory, and the University of Washington.

Appendix 1. Varying Radius

In Section 3, we used a fixed 0.7 Mpc radius to measure blue/spiral fractions among cluster galaxies since it was difficult to measure virial radius for relatively poor clusters in our sample from the SDSS imaging data. However it is known that virial radius changes according to cluster richness; i.e. richer clusters have larger virial radius than poorer clusters. Therefore using a fixed radius could bring some bias associated with cluster richness. In this section we try to rectify this problem using cluster richness to calculate virial radius under a simple assumption. We assume that our cluster richness (number of galaxies between $M_{r^*} = -24.0$ and $M_r = -19.44$ within 0.7 Mpc after fore/background subtraction) is proportional to volume of a cluster, and therefore proportional to *radius*³. Since richness is a relatively easy parameter to measure from the imaging data, we use the following equation to calculate radius for each cluster.

$$radius = 0.7 \times (Richness/32)^{1/3} \tag{A1}$$

where median richness of our sample cluster is 32. The coefficient of the equation is adjusted so that median clusters in our sample have radius of 0.7 Mpc, which corresponds to the mean radius used in Butcher et al. (1978, 1984) and Margoniner et al. (2000, 2001). The distribution of radius calculated in this way is presented in figure 12. As expected it has a peak at 0.7 Mpc. Using this varying radius, we re-calculated all figures in Section 3. Sample clusters

are still required to have more than 25 galaxies after fore/background subtraction within the new radius. Therefore the number of sample clusters are somewhat reduced to 413 clusters. Results are presented in figures 13-15. Reassuringly, all figures have the same trend as presented in Section 3. Therefore the discussion in Section 4 still holds. Although it is ideal to use virial radius to measure blue/spiral fractions of clusters, we regard that our analysis using fixed 0.7 Mpc radius is not hampered to the extent where our main conclusions change.

Appendix 2. Errors on Blue/Late Type Fractions

In this section we summarize how we derived eq. (2) to calculate errors on blue/late type fractions. As a starting point, we assume the following.

- Number of galaxies in a cluster region (N_{c+f}^{all}) follows Poisson statistics.
- Number of galaxies in a certain area of field region (N_f^{all}) follows Poisson statistics.
- N_{c+f}^* and N_f^* are independent of each other.
- Number of blue/late type galaxies in a cluster region (N_{c+f}^{late}) is strongly correlated with number of all galaxies in that region (N_{c+f}^{all}).
- Number of blue/late type galaxies in a certain field region (N_f^{late}) is strongly correlated with number of all galaxies in that region (N_f^{all}).

And we clarify the definition of our notation. In this appendix, δA means a deviation of a sampled value from an expectation value, $E(A)$.

$\delta A = A - E(A)$, where A is each data value.

$E(A)$ and δA satisfy the following relations.

$E(\delta A) = 0$, $E(\delta A)^2 = \sigma^2$, and if A and B are independent, $E(\delta A \delta B) = 0$. Note that the equation 2 is not a deviation of a single sample but the expectation value estimated from the sample, and should be written as $E(\delta f_{late}^2)$ if we write rigidly.

Under these assumptions, the error of late type fraction, δf_{late} , become

$$\delta f_{late}^2 = (X/Y)^2 \times ((\delta X^2/X^2) + (\delta Y^2/Y^2) - 2(\delta X \delta Y / XY)), \quad (A2)$$

where $X = N_{c+f}^{late} - N_f^{late}$, $Y = N_{c+f}^{all} - N_f^{all}$, and $f_{late} = X/Y$.

Since N_{c+f}^{all} and N_f^{all} follow Poisson statistics, and they are independent.

$$E(\delta Y^2) = N_{c+f}^{all} + N_f^{all} \quad (A3)$$

Similarly, when N_{c+f}^{all} follows Poisson statistics, N_{c+f}^{late} also follows Poisson statistics since $N_{c+f}^{late} \sim N_{c+f}^{all} \times f_{late}$. Therefore,

$$E(\delta X^2) = N_{c+f}^{late} + N_f^{late}. \quad (A4)$$

Deriving the cross term at the end of the equation is not so straightforward. The cross term is expanded as

$$\delta X \delta Y = \delta(N_{c+f}^{late} - N_f^{late}) \delta(N_{c+f}^{all} - N_f^{all}) \quad (A5)$$

$$= (\delta(N_{c+f}^{late}) - \delta(N_f^{late}))(\delta(N_{c+f}^{all}) - \delta(N_f^{all})) \quad (A6)$$

$$= \delta(N_{c+f}^{late})\delta(N_{c+f}^{all}) - \delta(N_f^{late})\delta(N_{c+f}^{all}) - \delta(N_{c+f}^{late})\delta(N_f^{all}) + \delta(N_f^{late})\delta(N_f^{all}) \quad (A7)$$

Since we assume N_f^{late} and N_{c+f}^{all} , N_{c+f}^{all} and N_f^{late} are both independent,

$$E(-\delta(N_f^{late})\delta(N_{c+f}^{all})) = 0 \quad (A8)$$

and

$$E(-\delta(N_{c+f}^{late})\delta(N_f^{all})) = 0. \quad (A9)$$

Therefore,

$$E(\delta X \delta Y) = E(\delta(N_{c+f}^{late})\delta(N_{c+f}^{all}) + \delta(N_f^{late})\delta(N_f^{all})) \quad (A10)$$

Since we assume that N_{c+f}^{late} and N_{c+f}^{all} , or N_f^{late} and N_f^{all} strongly correlate, we can approximate that

$$E(\delta(N_{c+f}^{late})\delta(N_{c+f}^{all})) = \sigma(N_{c+f}^{late})\sigma(N_{c+f}^{all}) = \sqrt{N_{c+f}^{late}}\sqrt{N_{c+f}^{all}} \quad (A11)$$

and,

$$E(\delta(N_f^{late})\delta(N_f^{all})) = \sigma(N_f^{late})\sigma(N_f^{all}) = \sqrt{N_f^{late}}\sqrt{N_f^{all}} \quad (A12)$$

Therefore we obtain,

$$E(\delta X \delta Y) = \sqrt{N_{c+f}^{late}}\sqrt{N_{c+f}^{all}} + \sqrt{N_f^{late}}\sqrt{N_f^{all}} \quad (A13)$$

By substituting eq. (A13) for $\delta X \delta Y$ in eq. (A2), we derive eq. (2).

However this is not the only way to estimate the error. Actually, the correlation between N_f^{late} and N_f^{all} is not so obvious since late type fraction in the field and that in the cluster region might be different. Although we regard the difference is so small that we can assume the eq.(A12), if we assume that N_f^{late} , $N_f^{early}(=N_f^{all}-N_f^{late})$, N_{c+f}^{late} , and $N_{c+f}^{early}(=N_{c+f}^{all}-N_{c+f}^{late})$ are independent, we derive,

$$E(\delta(N_{c+f}^{late})\delta(N_{c+f}^{all})) = E(\delta(N_{c+f}^{late})(\delta(N_{c+f}^{late}) + \delta(N_{c+f}^{early}))) = \sigma(N_{c+f}^{late})^2 = N_{c+f}^{late} \quad (A14)$$

and,

$$\delta(N_f^{late})\delta(N_f^{all}) = \sigma(N_f^{late})^2 = N_f^{late}. \quad (A15)$$

Then, the expectation value of $\delta X \delta Y$ becomes,

$$E(\delta X \delta Y) = N_{c+f}^{late} + N_f^{late} \quad (A16)$$

In this case, eq. (2) becomes,

$$E(\delta f_{late}) = f_{late} \times \sqrt{\frac{N_{c+f}^{late} + N_f^{late}}{(N_{c+f}^{late} - N_f^{late})^2} + \frac{N_{c+f}^{all} + N_f^{all}}{(N_{c+f}^{all} - N_f^{all})^2} - \frac{2(N_{c+f}^{late} + N_f^{late})}{(N_{c+f}^{late} - N_f^{late})(N_{c+f}^{all} - N_f^{all})}} \quad (A17)$$

References

- Abadi, M. G., Moore, B., & Bower, R. G. 1999, MNRAS, 308, 947
- Abell, G. 1958, APJS, 3, 211
- Abell, G., Corwin, H. & Olowin, R. 1989, APJS, 70, 1
- Abraham, R. G., van den Bergh, S., Glazebrook, K., Ellis, R. S., Santiago, B. X., Surma, P., & Griffiths, R. E. 1996, ApJS, 107, 1
- Abraham, R. G., Valdes, F., Yee, H. K. C., & van den Bergh, S. 1994, ApJ, 432, 75
- Abraham, R. G. et al. 1996, ApJ, 471, 694
- Abraham, R. G. & van den Bergh, S. 2001, Science, 293, 1273
- Allen, S. W. & Fabian, A. C. 1998, MNRAS, 297, L57
- Allington-Smith, J. R., Ellis, R., Zirbel, E. L., & Oemler, A. J. 1993, ApJ, 404, 521
- Andreon, S. & Ettori, S. 1999, ApJ, 516, 647
- Annis, J. et al. 2002 *in preparation*
- Arnaud, M. & Evrard, A. E. 1999, MNRAS, 305, 631
- Bahcall, N. A. 1974, ApJ, 193, 529
- Bahcall, N. A. 1977, ApJL, 218, L93
- Bahcall, N. A. et al. 2002 *in preparation*
- Balogh, M. L., Morris, S. L., Yee, H. K. C., Carlberg, R. G., & Ellingson, E. 1997, ApJL, 488, L75
- Balogh, M. L., Morris, S. L., Yee, H. K. C., Carlberg, R. G., & Ellingson, E. 1999, ApJ, 527, 54
- Balogh, M. L., Navarro, J. F., & Morris, S. L. 2000, ApJ, 540, 113
- Balogh, M. L., Christlein, D., Zabludoff, A. I., & Zaritsky, D. 2001, ApJ, 557, 117
- Balogh, M., Bower, R. G., Smail, I., Ziegler, B. L., Davies, R. L., Gaztelu, A., & Fritz, A. 2002, MNRAS, 337, 256
- Bekki, K. 1998, ApJL, 502, L133
- Bekki, K., Shioya, Y., & Couch, W. J. 2001, ApJL, 547, L17
- Bekki, K., Couch, W. J., & Shioya, Y. 2002, ApJ, 577, 651
- Binggeli, B., Sandage, A., & Tammann, G. A. 1988, ARA&A, 26, 509
- Binney, J., & Tremaine, S. 1987, Galactic Dynamics (Princeton: Princeton Univ. Press)
- Blanton, M. R. et al. 2001, AJ, 121, 2358
- Blanton, M.R., Lupton, R.H., Maley, F.M., Young, N., Zehavi, I., and Loveday, J. 2002, AJ, submitted
- Bower, R. G., Bohringer, H., Briel, U. G., Ellis, R. S., Castander, F. J., & Couch, W. J. 1994, MNRAS, 268, 345
- Boyce, P. J., Phillipps, S., Jones, J. B., Driver, S. P., Smith, R. M., & Couch, W. J. 2001, MNRAS, 328, 277.
- Bothun, G. D. & Dressler, A. 1986, ApJ, 301, 57
- Butcher, H. & Oemler, A. 1978, ApJ, 226, 559
- Butcher, H. & Oemler, A. 1984, ApJ, 285, 426
- Byrd, G. & Valtonen, M. 1990, ApJ, 350, 89
- Cavaliere, A., Menci, N., & Tozzi, P. 1997, ApJL, 484, L21
- Couch, W. J., Ellis, R. S., Sharples, R. M., & Smail, I. 1994, ApJ, 430, 121
- Couch, W. J., Barger, A. J., Smail, I., Ellis, R. S., & Sharples, R. M. 1998, ApJ, 497, 188

Cowie, L. L., Songaila, A., & Barger, A. J. 1999, *AJ*, 118, 603

David, L. P., Slyz, A., Jones, C., Forman, W., Vrtiliek, S. D., & Arnaud, K. A. 1993, *ApJ*, 412, 479

Diaferio, A., Kauffmann, G., Balogh, M.L., White, S.D.M., Schade, D. & Ellingson, E. 2001, *MNRAS*, 323, 999.

Doi, M., Fukugita, M., & Okamura, S. 1993, *MNRAS*, 264, 832

Dressler, A. 1980, *ApJ*, 236, 351

Dressler, A. & Gunn, J. E. 1992, *ApJS*, 78, 1

Dressler, A. et al. 1997, *ApJ*, 490, 577

Dressler, A., Smail, I., Poggianti, B. M., Butcher, H., Couch, W. J., Ellis, R. S., & Oemler, A. J. 1999, *ApJS*, 122, 51

Edge, A. C. & Stewart, G. C. 1991, *MNRAS*, 252, 414

Eisenstein, D. J. et al. 2001, *AJ*, 122, 2267

Ellingson, E., Lin, H., Yee, H. K. C., & Carlberg, R. G. 2001, *ApJ*, 547, 609

Evrard, A. E. 1991, *MNRAS*, 248, 8P

Fairley, B. W., Jones, L. R., Wake, D. A., Collins, C. A., Burke, D. J., Nichol, R. C., & Romer, A. K. 2002, *MNRAS*, 330, 755

Farouki, R. & Shapiro, S. L. 1980, *ApJ*, 241, 928

Fasano, G., Poggianti, B. M., Couch, W. J., Bettoni, D., Kjærgaard, P., & Moles, M. 2000, *ApJ*, 542, 673

Finoguenov, A., Briel, U.G., Henry, J.P., 2003, submitted to *A&A*

Fujita, Y. 1998, *ApJ*, 509, 587

Fujita, Y. & Nagashima, M. 1999, *ApJ*, 516, 619

Fujita, Y. 2001, *ApJ*, 550, 612

Fukugita, M., Shimasaku, K., & Ichikawa, T. 1995, *PASP*, 107, 945

Fukugita, M., Ichikawa, T., Gunn, J. E., Doi, M., Shimasaku, K., & Schneider, D. P. 1996, *AJ*, 111, 1748.

Gal, R. R., de Carvalho, R. R., Brunner, R., Odewahn, S. C., & Djorgovski, S. G. 2000, *AJ*, 120, 540

Garilli, B., Bottini, D., Maccagni, D., Carrasco, L., & Recillas, E. 1996, *ApJS*, 105, 191

Goto, T. et al. 2002a, *AJ*, 123, 1807.

Goto, T., Okamura, S. & Brinkman, J. 2002b, *PASJ*, 54, 4

Gladders, M. D. & Yee, H. K. C. 2000, *AJ*, 120, 2148

Gunn, J. E. & Gott, J. R. I. 1972, *ApJ*, 176, 1

Gunn, J.E., Carr, M., Rockosi, C., Sekiguchi, M., Berry, K., Elms, B., de Haas, E., Ivezić, Z. et al. 1998, *AJ*, 116, 3040

Gunn, J.E., Hoessel, J.G., & Oke, J.B. 1986, *ApJ*, 306, 30.

Hammer, F., Flores, H., Lilly, S. J., Crampton, D., Le Fevre, O., Rola, C., Mallen-Ornelas, G., Schade, D., & Tresse, L. 1997, *ApJ*, 481, 49

Henry, J. P. & Arnaud, K. A. 1991, *ApJ*, 372, 410

Hogg, D. W., Finkbeiner, D. P., Schlegel, D. J., & Gunn, J. E. 2001, *AJ*, 122, 2129

Icke, V. 1985, *A&A*, 144, 115

Jones, C. & Forman, W. 1978, *ApJ*, 224, 1

- Jones, C. & Forman, W. 1999, ApJ, 511, 65
- Kauffmann, G. 1995, MNRAS, 274, 153
- Kent, S. M. 1981, ApJ, 245, 805
- Kim, R. S. J. et al. 2002, AJ, 123, 20
- Kodama, T., Smail, I., Nakata, F., Okamura, S., & Bower, R. G. 2001, ApJL, 562, L9
- Kodama, T. & Bower, R. G. 2001, MNRAS, 321, 18
- Kodama, T. & Smail, I. 2001, MNRAS, 326, 637
- Lahav, O. et al. 1995, Science, 267, 859
- Larson, R. B., Tinsley, B. M., & Caldwell, C. N. 1980, ApJ, 237, 692
- Lavery, R. J. & Henry, J. P. 1988, ApJ, 330, 596
- Lea, S. M. & Henry, J. P. 1988, ApJ, 332, 81
- Lilly, S. J., Le Fevre, O., Hammer, F., & Crampton, D. 1996, ApJL, 460, L1
- Lilly, S., Schade, D., Ellis, R., Le Fevre, O., Brinchmann, J., Tresse, L., Abraham, R., Hammer, F., et al. 1998, ApJ, 500, 75
- Lin, H., Yee, H. K. C., Carlberg, R. G., Morris, S. L., Sawicki, M., Patton, D. R., Wirth, G., & Shepherd, C. W. 1999, ApJ, 518, 533
- Loveday, J., Peterson, B. A., Efstathiou, G., & Maddox, S. J. 1992, ApJ, 390, 338
- Lupton, R. H., Gunn, J. E., & Szalay, A. S. 1999, AJ, 118, 1406
- Lupton, R. H., Gunn, J. E., Ivezić, Z., Knapp, G. R., Kent, S., & Yasuda, N. 2001, Astronomical Data Analysis Software and Systems X, ASP Conference Proceedings, Vol. 238. Edited by F. R. Harnden, Jr., Francis A. Primini, and Harry E. Payne. San Francisco: Astronomical Society of the Pacific, ISSN: 1080-7926, 2001., p.269, 10, 269
- Lupton, R. et al. 2002, *in preparation*
- Madau, P., Ferguson, H. C., Dickinson, M. E., Giavalisco, M., Steidel, C. C., & Fruchter, A. 1996, MNRAS, 283, 1388
- Makino, J. & Hut, P. 1997, ApJ, 481, 83
- Mamon, G. A. 1992, ApJL, 401, L3
- Margoniner, V. E. & de Carvalho, R. R. 2000, AJ, 119, 1562
- Margoniner, V. E., de Carvalho, R. R., Gal, R. R., & Djorgovski, S. G. 2001, ApJL, 548, L143
- Markevitch, M. 1998, ApJ, 504, 27
- Marzke, R. O., Geller, M. J., Huchra, J. P., & Corwin, H. G. 1994, AJ, 108, 437
- Marzke, R. O. & da Costa, L. N. 1997, AJ, 113, 185
- Marzke, R. O., da Costa, L. N., Pellegrini, P. S., Willmer, C. N. A., & Geller, M. J. 1998, ApJ, 503, 617
- Metevier, A. J., Romer, A. K., & Ulmer, M. P. 2000, AJ, 119, 1090
- Mihos, J. C. 1995, ApJL, 438, L75
- Miller, C. J. et al. astro-ph/9912362
- Miller, C. J. et al. 2002 *in preparation*
- Mitchell, R. J., Ives, J. C., & Culhane, J. L. 1977, MNRAS, 181, 25P
- Mo, H. J. & Mao, S. 2002, MNRAS, 333, 768
- Moore, B., Katz, N., Lake, G., Dressler, A., & Oemler, A. 1996, Nature, 379, 613

Moore, B., Lake, G., Quinn, T., & Stadel, J. 1999, MNRAS, 304, 465
Morgan, W. W. 1958, PASP, 70, 364
Morgan, W. W. 1959, PASP, 71, 394
Newberry, M. V., Kirshner, R. P., & Boroson, T. A. 1988, ApJ, 335, 629
Oh, S.P. & Benson, A.J. 2003, submitted to MNRAS
Ostriker, J. P. 1980, Comments on Astrophysics, 8, 177
Pier, J. R., Munn, J. A., Hindsley, R. B., Hennessy, G. S., Kent, S. M., Lupton, R. H., & Ivezić, Ž. 2003, AJ, 125, 1559
Poggianti, B. M., Smail, I., Dressler, A., Couch, W. J., Barger, A. J., Butcher, H., Ellis, R. S., & Oemler, A. J. 1999, ApJ, 518, 576
Quilis, V., Moore, B., & Bower, R. 2000, Science, 288, 1617
Rakos, K. D. & Schombert, J. M. 1995, ApJ, 439, 47
Reichart, D. E., Castander, F. J., & Nichol, R. C. 1999, ApJ, 516, 1
Schade, D., Lilly, S. J., Le Fevre, O., Hammer, F., & Crampton, D. 1996, ApJ, 464, 79
Schlegel, D. J., Finkbeiner, D. P., & Davis, M. 1998, ApJ, 500, 525
Scranton, R. et al. 2002 *in preparation*
Sellwood, J. A. & Carlberg, R. G. 1984, ApJ, 282, 61
Shimasaku, K. et al. 2001, AJ, 122, 1238
Shioya, Y., Bekki, K., Couch, W. J., & De Propris, R. 2002, ApJ, 565, 223
Smail, I., Dressler, A., Couch, W. J., Ellis, R. S., Oemler, A. J., Butcher, H., & Sharples, R. M. 1997, ApJS, 110, 213
Smail, I., Edge, A. C., Ellis, R. S., & Blandford, R. D. 1998, MNRAS, 293, 124
Smith, J. A. et al. 2002, AJ, 123, 2121
Spitzer, L. J. & Baade, W. 1951, ApJ, 113, 413
Stevens, I. R., Acreman, D. M., & Ponman, T. J. 1999, MNRAS, 310, 663
Strauss, M. A. et al. 2002, AJ, 124, 1810
Strateva, I. et al. 2001, AJ, 122, 1861
Stoughton, C. et al. 2002, AJ, 123, 485
Sullivan, M., Treyer, M. A., Ellis, R. S., Bridges, T. J., Milliard, B., & Donas, J. ; 2000, MNRAS, 312, 442
Treyer, M. A., Ellis, R. S., Milliard, B., Donas, J., & Bridges, T. J. 1998, MNRAS, 300, 303
Valotto, C. A., Moore, B., & Lambas, D. G. 2001, ApJ, 546, 157
Valluri, M. 1993, ApJ, 408, 57
van den Bergh, S. 1976, ApJ, 206, 883
Vollmer, B., Cayatte, V., Balkowski, C., & Duschl, W. J. 2001, ApJ, 561, 708
Wang, Q. D. & Ulmer, M. P. 1997, MNRAS, 292, 920
White, D. A., Jones, C., & Forman, W. 1997, MNRAS, 292, 419
Wilson, G., Cowie, L. L., Barger, A. J., & Burke, D. J. 2002, AJ, 124, 1258
Wu, X., Xue, Y., & Fang, L. 1999, ApJ, 524, 22
Xue, Y. & Wu, X. 2000, ApJ, 538, 65

- Yagi, M., Kashikawa, N., Sekiguchi, M., Doi, M., Yasuda, N., Shimasaku, K., & Okamura, S. 2002, AJ, 123, 87
- Yagi, M., Kashikawa, N., Sekiguchi, M., Doi, M., Yasuda, N., Shimasaku, K., & Okamura, S. 2002, AJ, 123, 66
- Yee, H. K. C., Ellingson, E., & Carlberg, R. G. 1996, ApJS, 102, 269
- York, D. G. et al. 2000, AJ, 120, 1579

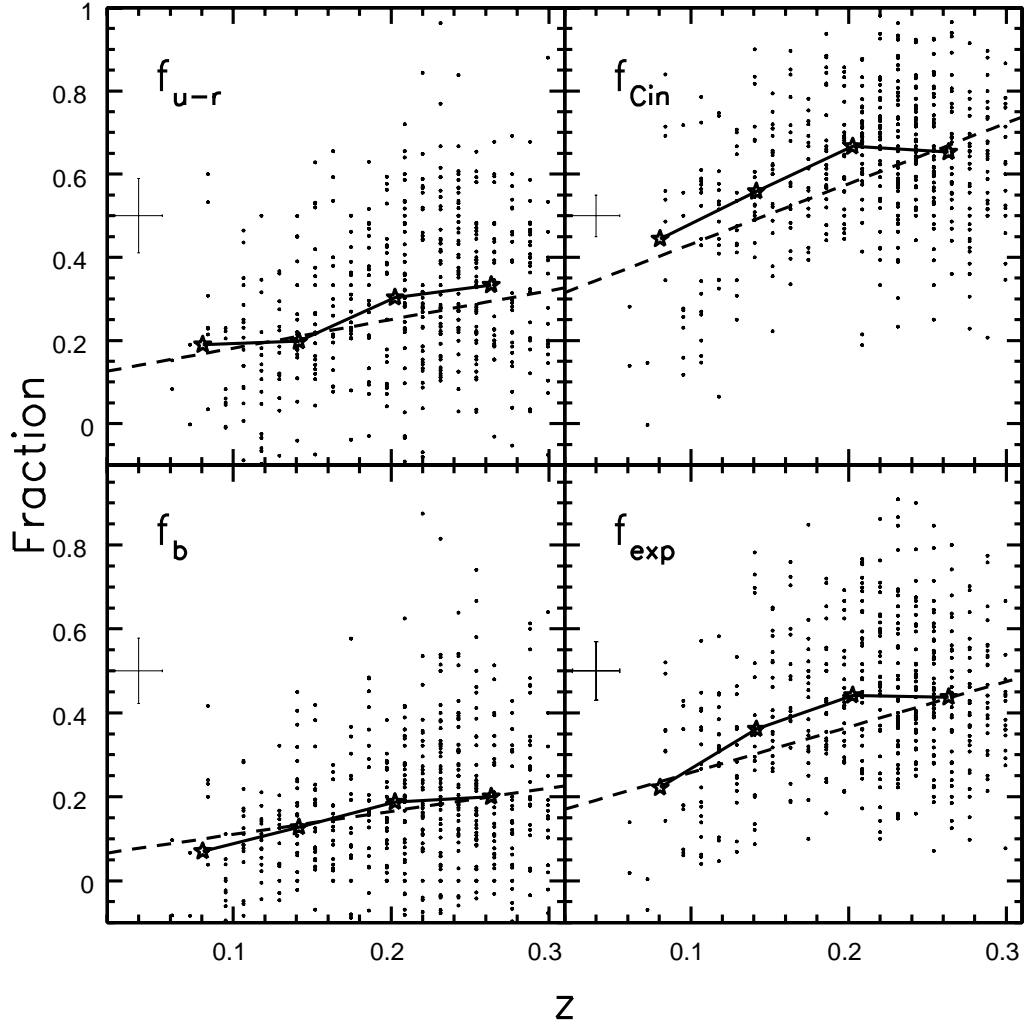


Fig. 1. Photometric and morphological Butcher-Oemler effect from the 514 SDSS Cut & Enhance clusters. f_b , f_{Cin} , f_{exp} and f_{u-r} are plotted against redshift. The dashed lines show the weighted least-squares fit to the data. The stars and solid lines show the median values. The median values of errors are shown in the upper left corners of each panel. The Spearman's correlation coefficients are shown in Table 1.

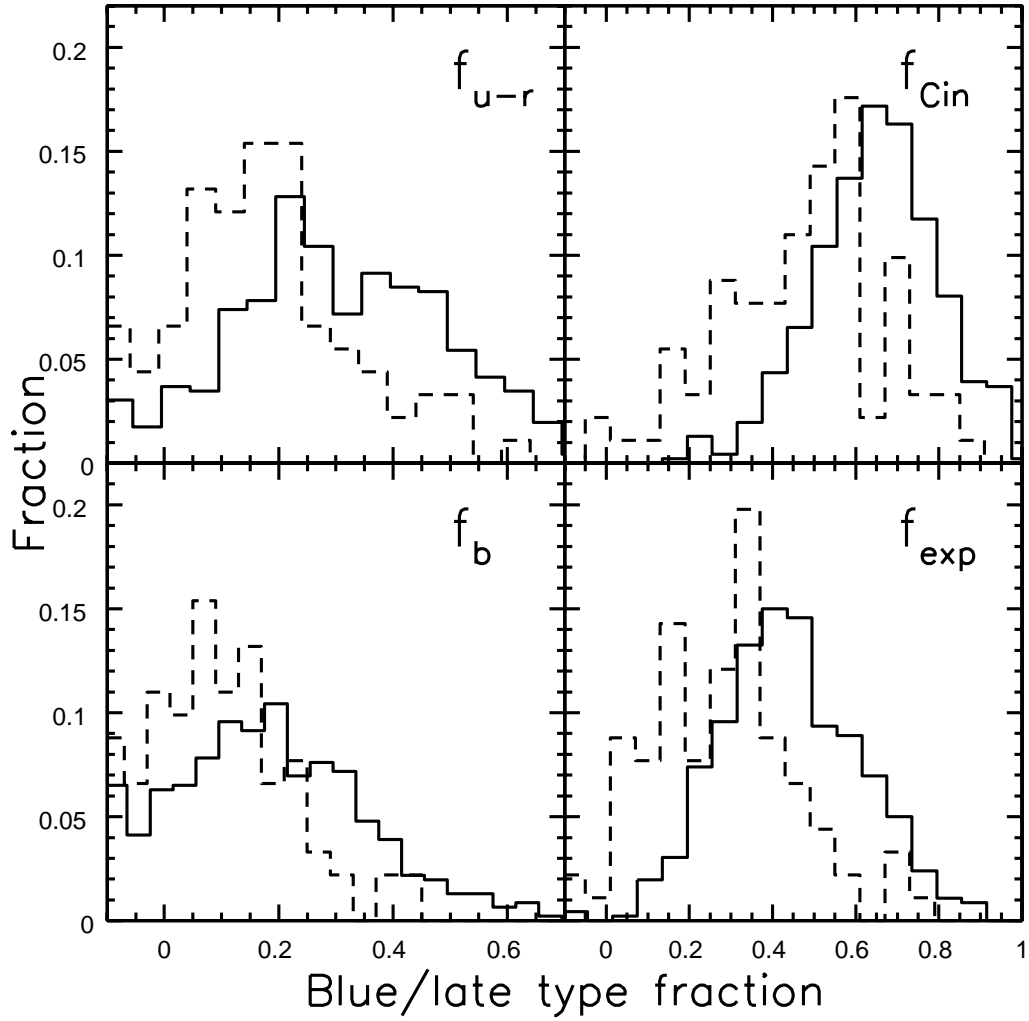


Fig. 2. Normalized distributions of late type fractions (f_b , f_{Cin} , f_{exp} and f_{u-r}). Dashed lines show distributions of lower redshift clusters ($z \leq 0.15$) and solid lines show ones of higher redshift clusters ($0.15 < z \leq 0.3$). The results of Kolomogorov-Smirnov tests are shown in Table 2. In all cases, Kolomogorov-Smirnov tests show the two distributions are significantly different.

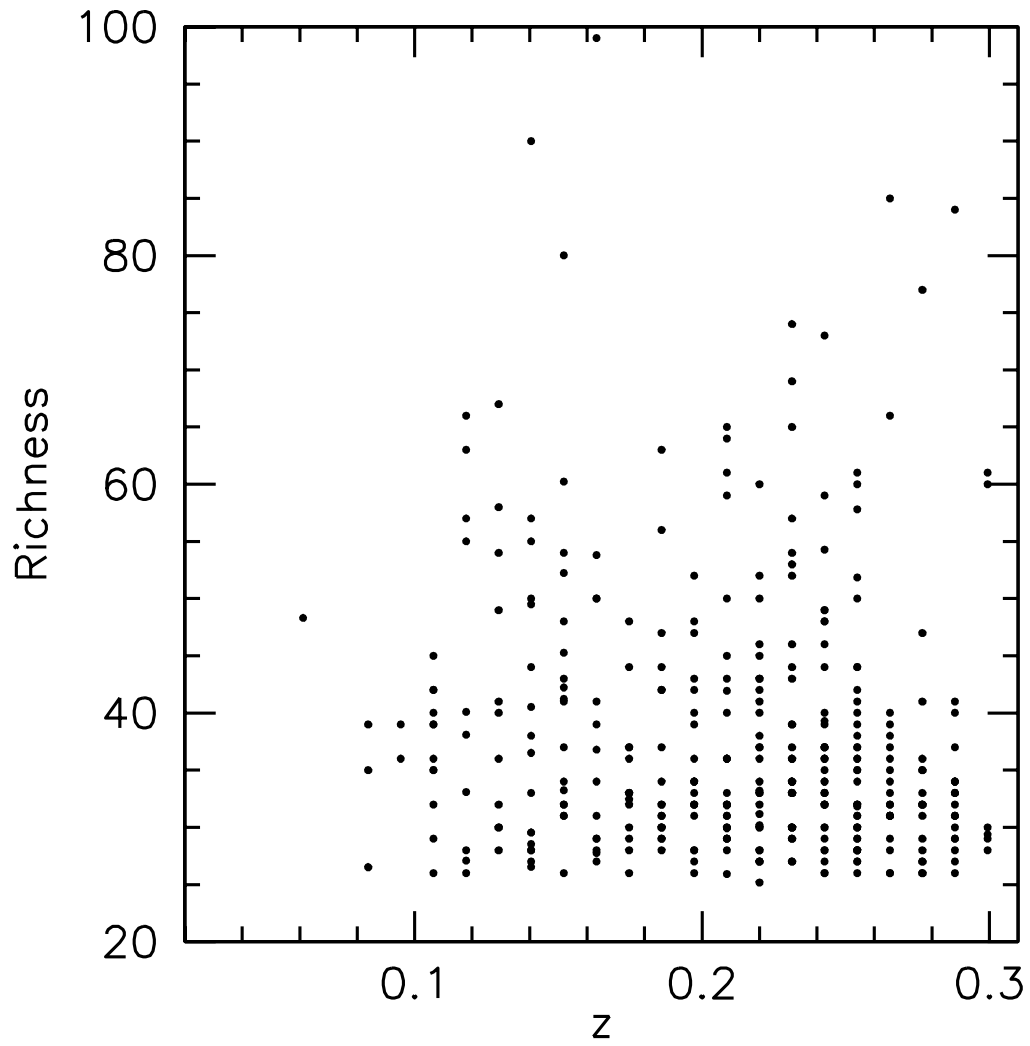


Fig. 3. Richness distribution as a function of redshift. Richnesses are measure as the number of galaxies brighter than $M_r = -19.44$ within 0.7 Mpc after fore/background subtraction.

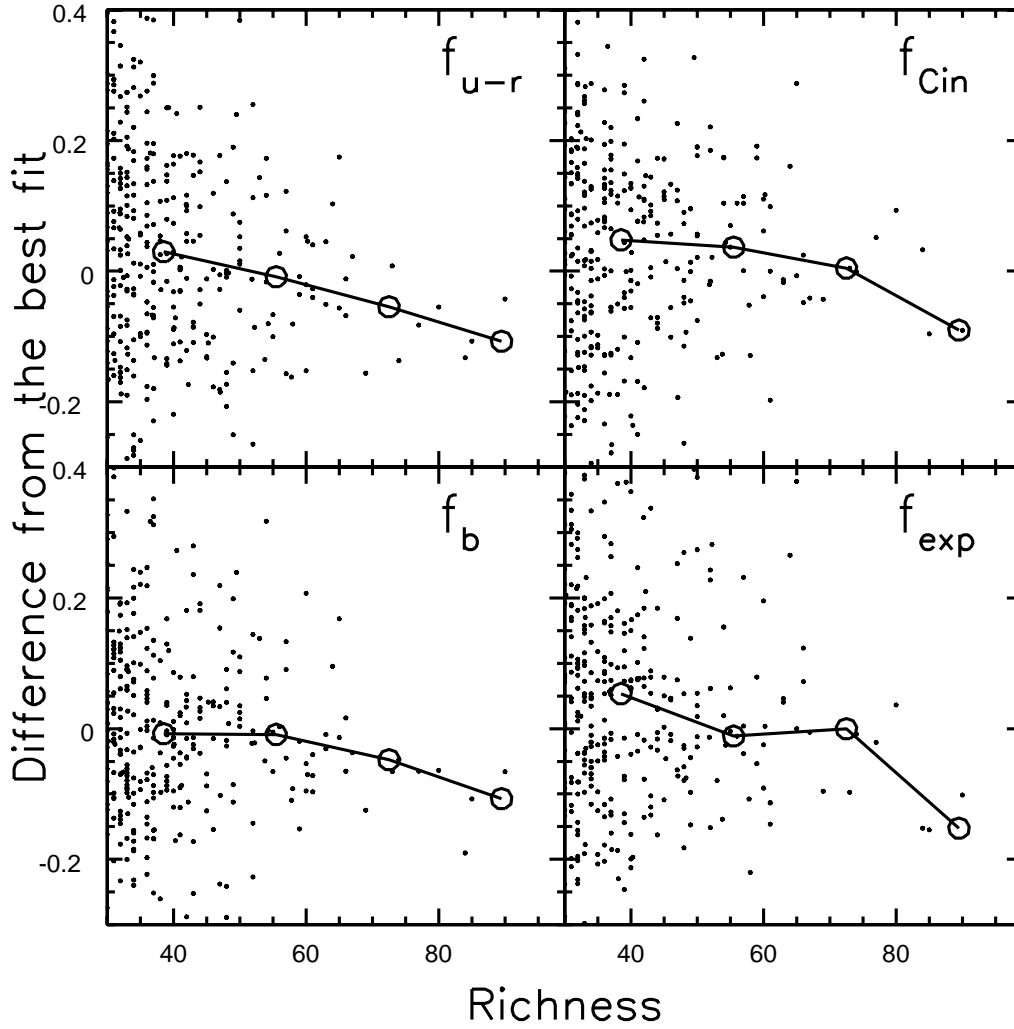


Fig. 4. The difference of the late type fractions from the best fit lines as a function of redshift are plotted against cluster richnesses. Solid lines and stars show the median values.

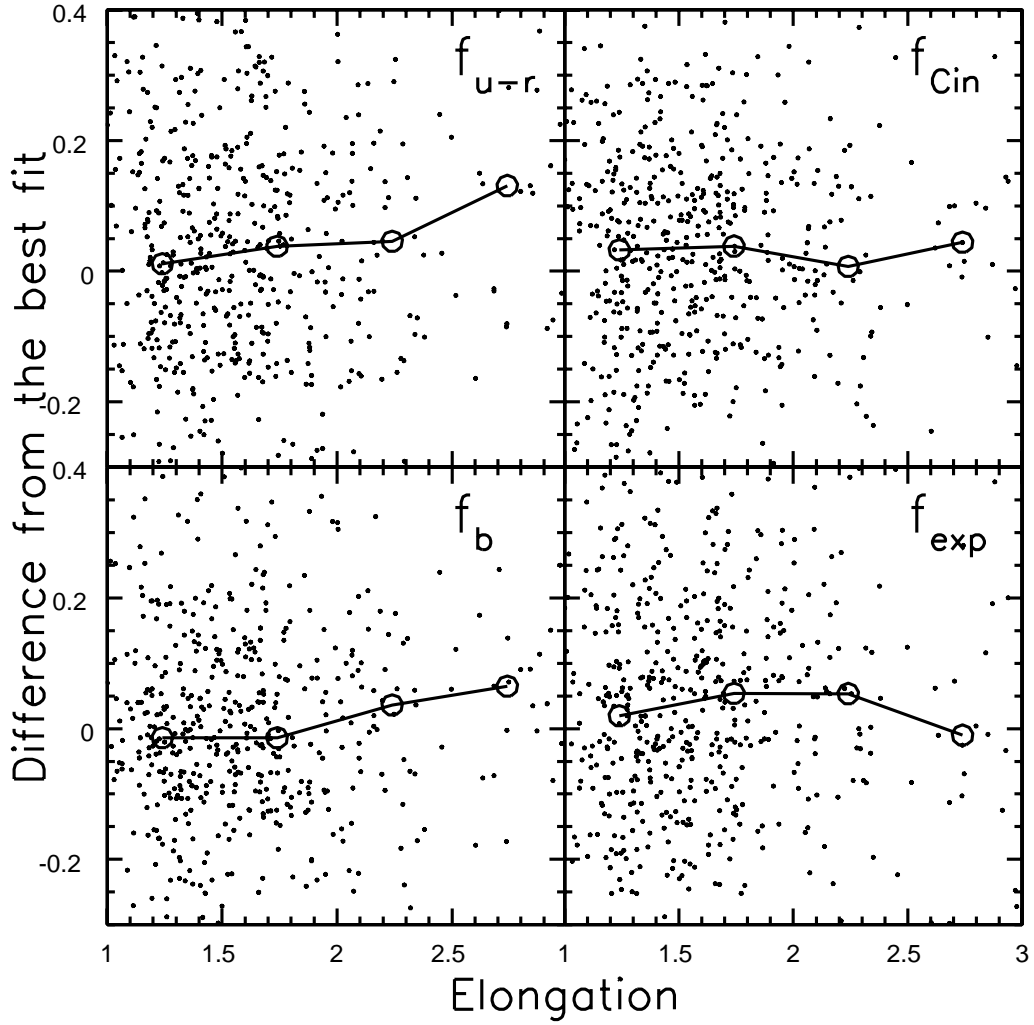


Fig. 5. The difference of late type fractions from the best fit lines as a function of redshift are plotted against cluster elongation, which was measured as a ratio of major axis to minor axis on a cluster detection map of Goto et al. (2002a). Solid lines and stars show median values.

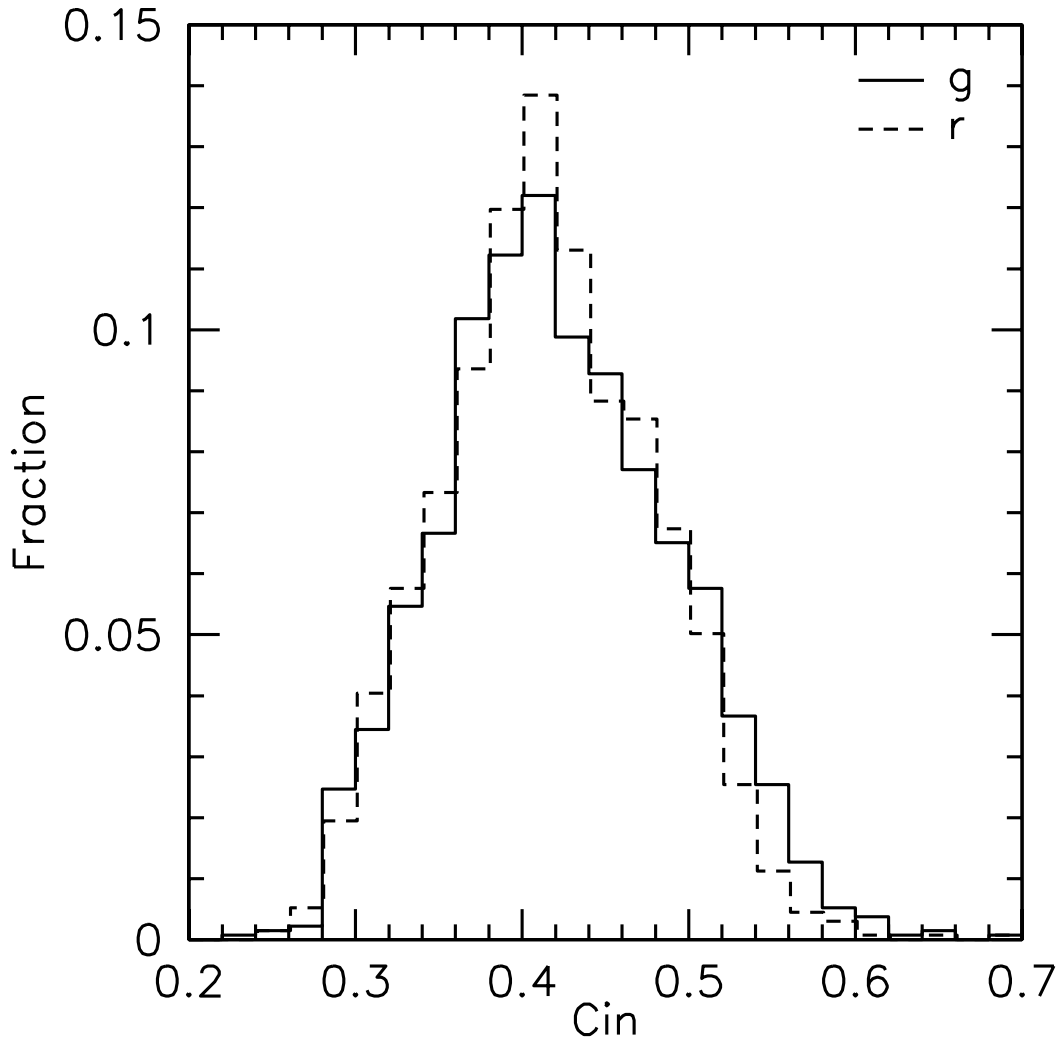


Fig. 6. The distribution of the inverse of the concentration index (C_{in}), defined as the ratio of Petrosian 50% flux radius to Petrosian 90% flux radius. The solid line shows the distribution of C_{in} measured in the g band image. The dashed line shows the distribution of C_{in} measured in the r band image. The difference between the g band and r band is marginal, assuring our usage of r band C_{in} in the right upper panel of Figure 1 from $z=0.02$ to $z=0.3$. The statistics are summarized in Table 4.

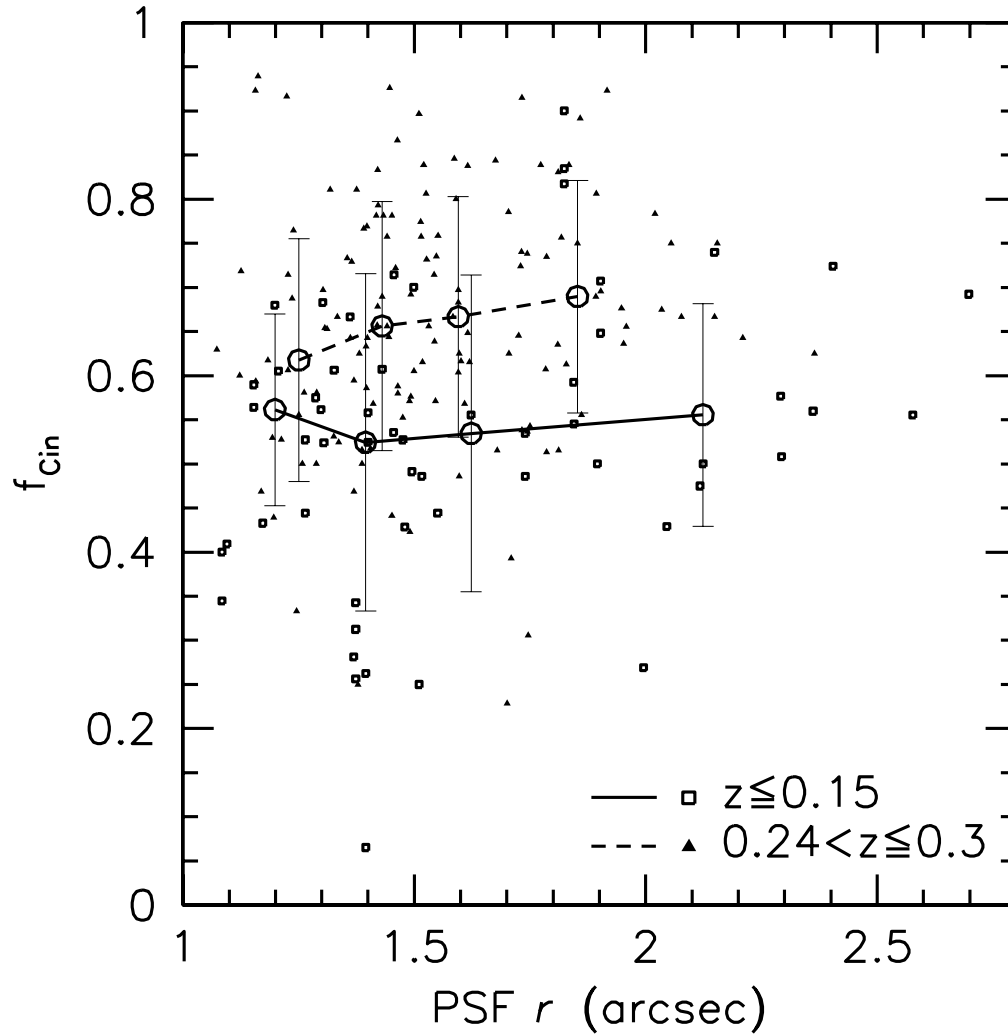


Fig. 7. The dependence of f_{Cin} on seeing. Open squares and solid lines show the distribution and medians of low z clusters ($z \leq 0.15$). Filled triangles and dashed lines show the distribution and medians of high z clusters ($0.24 < z \leq 0.3$). The median bins are chosen so that equal numbers of galaxies are included in each bin.

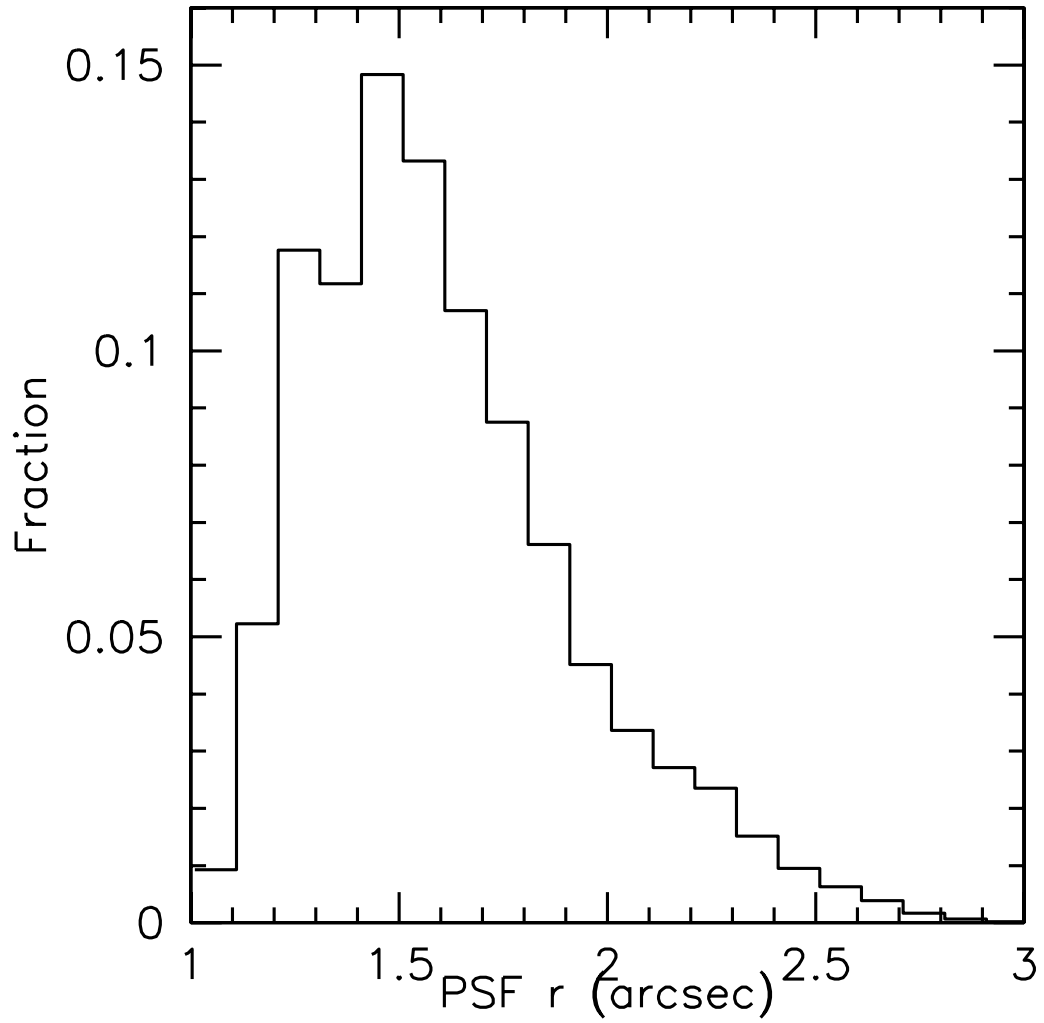


Fig. 8. The seeing distribution of all galaxies brighter than $r=21.5$. 87% of all galaxies have seeing better than 2.0 arcsec.

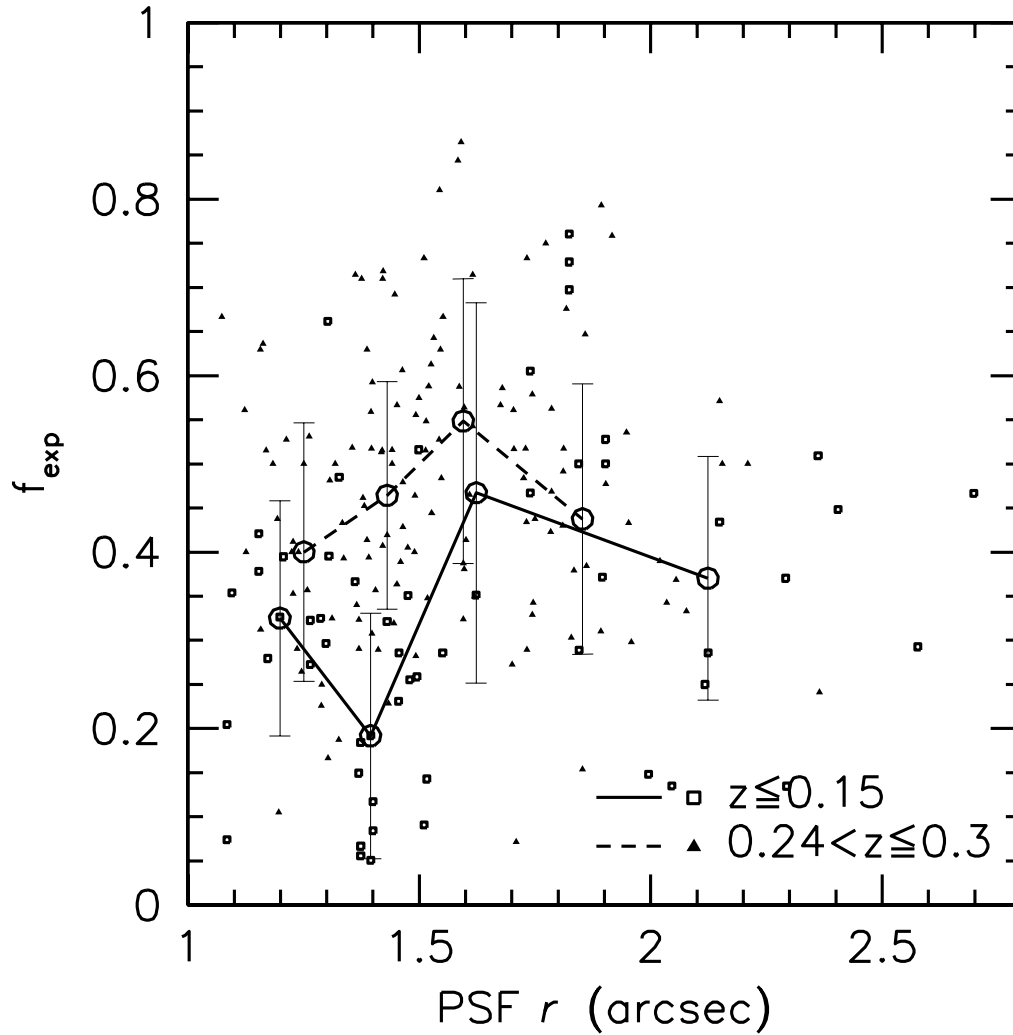


Fig. 9. The dependence of f_{exp} on seeing. Open squares and solid lines show the distribution and medians of low z clusters ($z \leq 0.15$). Filled triangles and dashed lines show the distribution and medians of high z clusters ($0.24 < z \leq 0.3$). Median bins are chosen so that equal numbers of galaxies are included in each bin. 1σ errors shown as vertical bars are more dominant. There is no significant trend with seeing.

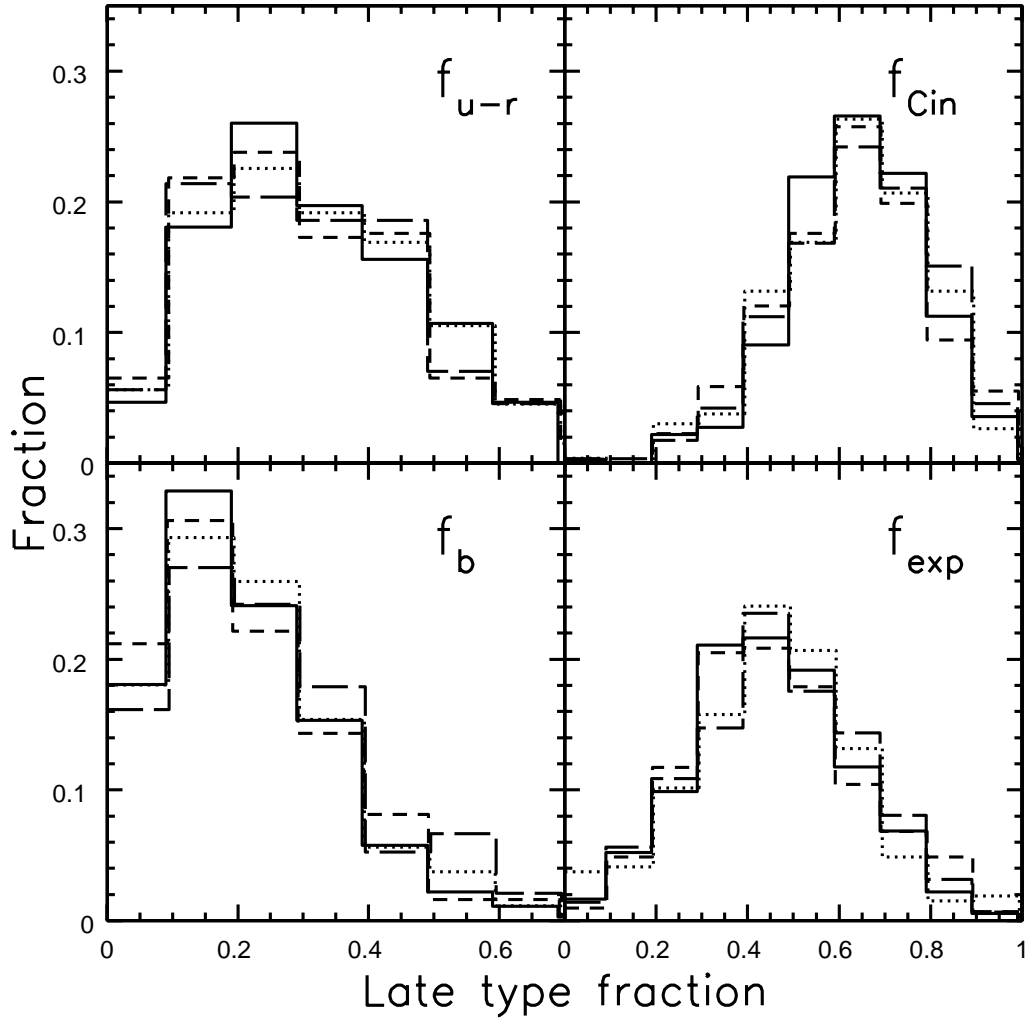


Fig. 10. Various systematic tests. Solid lines show distributions for 2.1-2.21 Mpc annular fore/background subtraction. Dashed lines show distributions for a global background subtraction. Dotted lines show distributions using $0.7/(1+z)$ Mpc radius assuming a standard cold dark matter cosmology. Long dashed lines show distributions using the brightest galaxy position as a cluster center. In none of the cases does a Kolomogorov-Smirnov test show significant difference between the distributions (significance to be different is less than 26% in all cases).

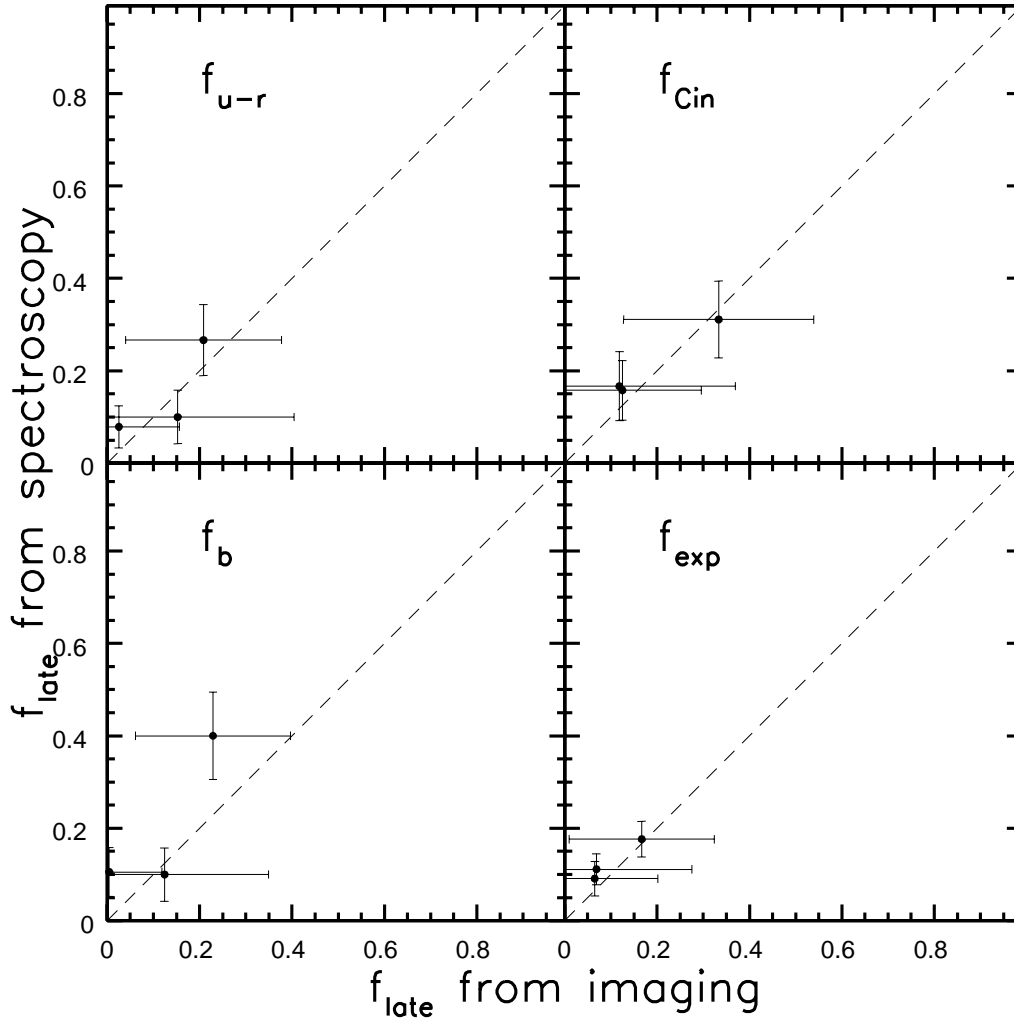


Fig. 11. Comparison with late-type fraction from spectroscopy. Late-type fractions measured using spectroscopic data are plotted against that from imaging data for three clusters with $z < 0.06$ (ABELL 295, RXC J0114.9+0024, and ABELL 957). Dashed lines are drawn to guide eyes. All points agree with each other within the error.

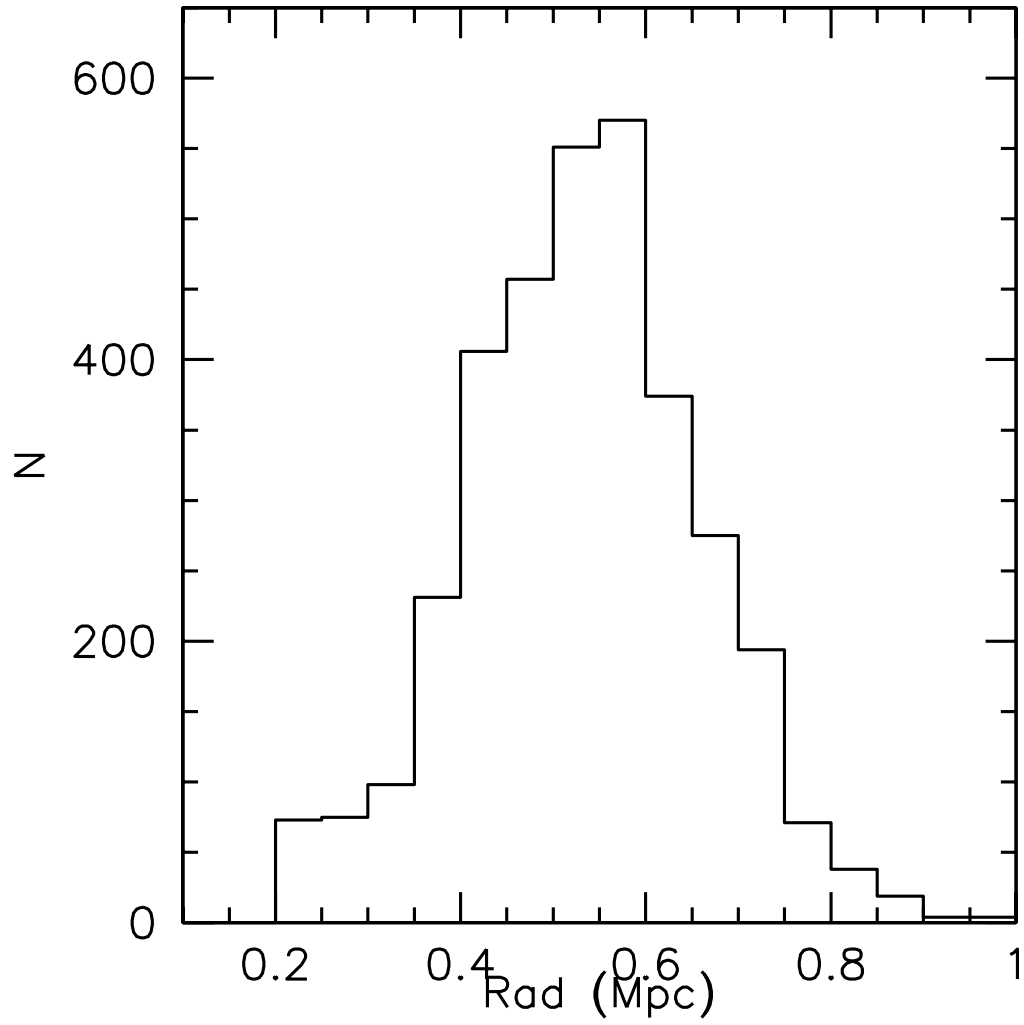


Fig. 12. Distribution of varying radius to measure blue/spiral fractions. It has a peak at 0.7 Mpc.

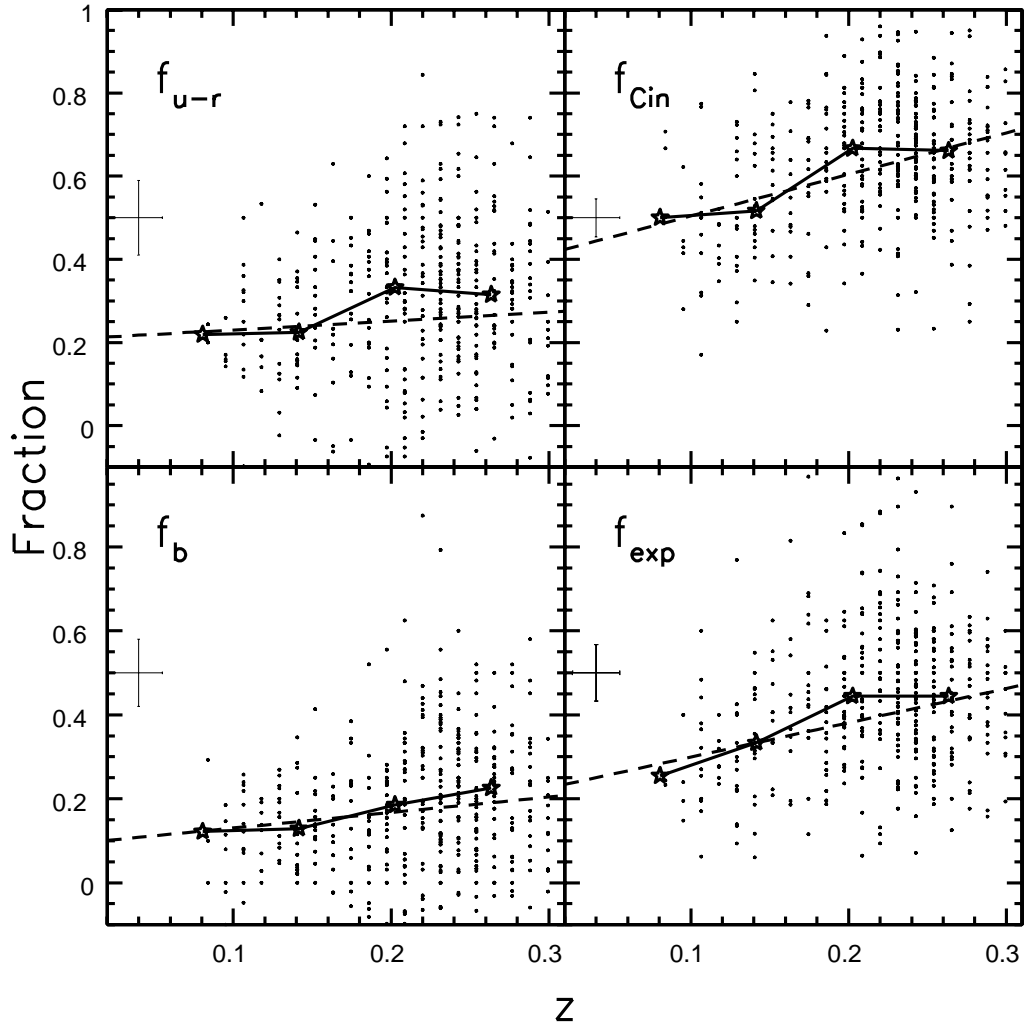


Fig. 13. The same as figure 1, but measured with varying radius.

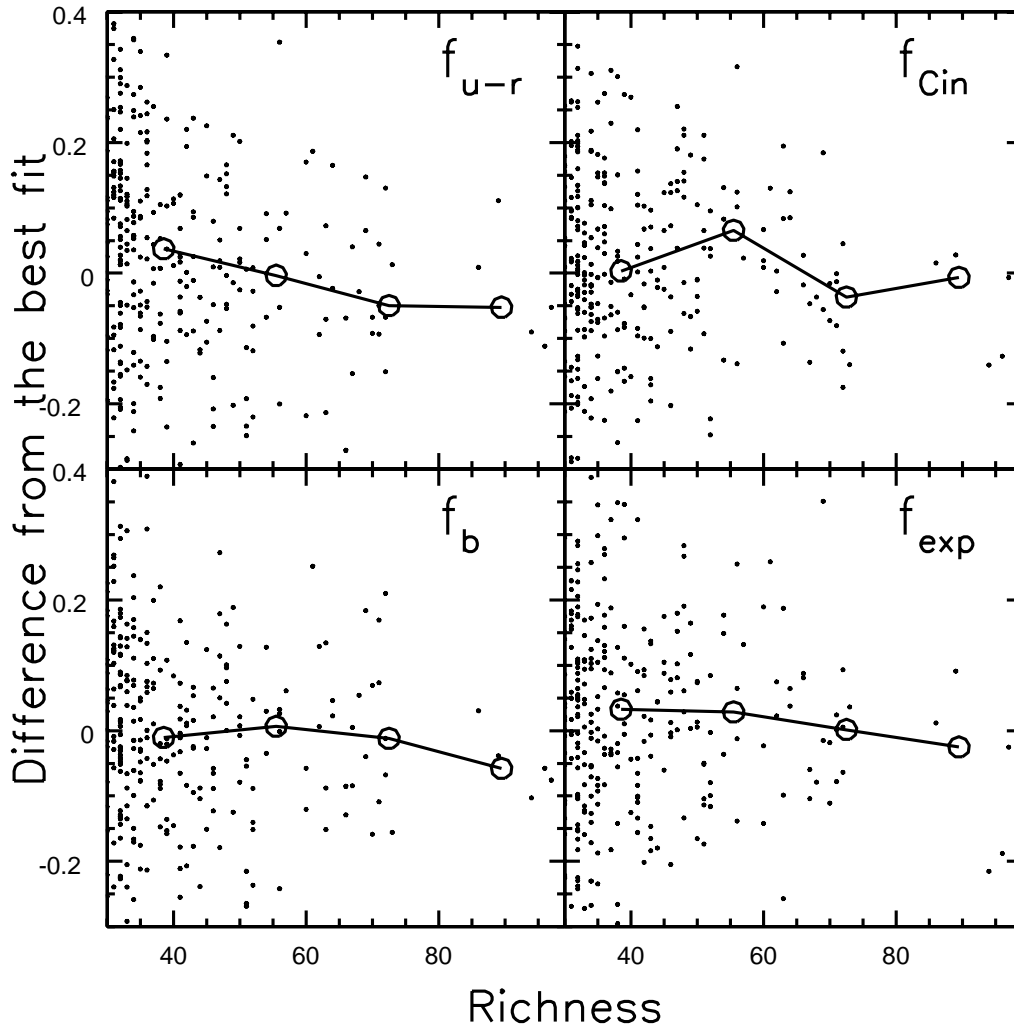


Fig. 14. The same as figure 4, but measured with varying radius.

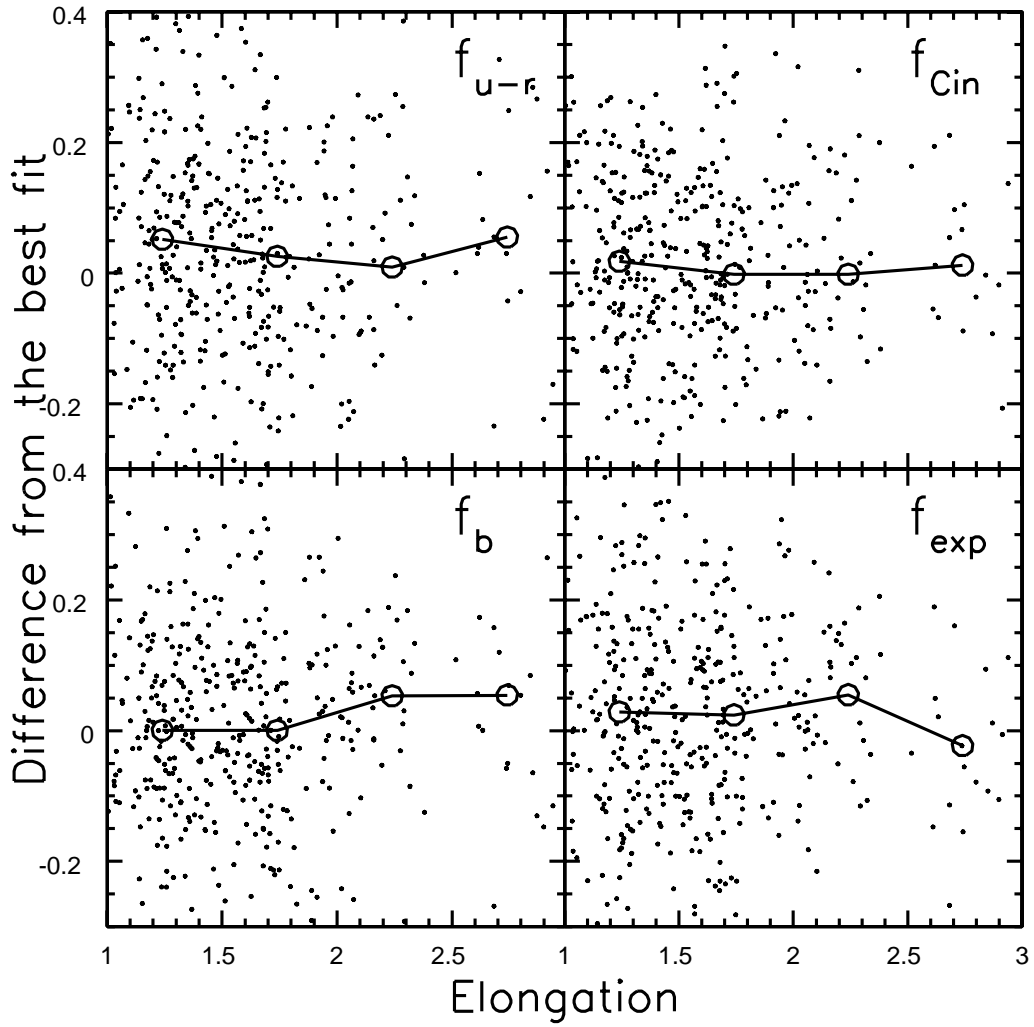


Fig. 15. The same as figure 5, but measured with varying radius.

Table 1. Spearman’s correlation coefficients between z and fractions of late type galaxies. 514 clusters with richness >25 are chosen as a sample.

	Correlation coefficient	Significance	N clusters
f_b	0.238	4.4×10^{-8}	514
f_{u-r}	0.234	7.6×10^{-8}	514
f_{exp}	0.194	9.6×10^{-6}	514
f_{Cin}	0.223	2.9×10^{-7}	514

Table 2. Significances in Kolomogorov-Smirnov tests between distributions for $z \leq 0.15$ and $0.15 < z < 0.3$. In all cases, Kolomogorov-Smirnov tests show the distributions for the lower redshift sample and the higher redshift sample are significantly different.

	Significance
f_b	2.9×10^{-3}
f_{u-r}	1.0×10^{-3}
f_{exp}	3.4×10^{-4}
f_{Cin}	2.9×10^{-3}

Table 3. Scatters in late-type fractions around the best-fit line are compared with median errors of late-type fraction calculated with equation (2)

	f_b	f_{u-r}	f_{exp}	f_{Cin}
Real scatter (1σ)	0.169	0.183	0.171	0.163
Error estimate	0.078	0.069	0.050	0.089

Table 4. Change in the fraction of galaxies with $C_{in} > 0.4$ (late type) in two different filters(g, r).

band	N($C_{in} > 0.4$)	N(total)	Percentage(%)
g	802	1336	60.0
r	787	1336	58.9
Difference	15	1336	1.1

Table 5. Change in the fraction of galaxies with exponential fit likelihood greater than de Vaucouleur likelihood (late type) in two different filters(g, r). Since we discard the galaxies with the same likelihood in this analysis, the total number of galaxies in the sample are different in g and r .

band	N(late)	N(late + early)	Percentage(%)
g	503	804	62.6
r	476	792	60.1
Difference	-	-	2.5